

# **LUBRICANT-INFUSED TITANIUM SURFACES**

**LUBRICANT-INFUSED TITANIUM SURFACES WITH  
SIMULTANEOUS ANTI-BIOFOULING AND TARGETED  
BINDING PROPERTIES**

By YUXI ZHANG, B.E.

A Thesis Submitted to the School of Graduate Studies in Fulfillment of the  
Requirements for the Degree Master of Applied Science

McMaster University ©Copyright by Yuxi Zhang, December 2019

McMaster University MASTER OF APPLIED SCIENCE, (2019)  
Hamilton, Ontario, Canada

TITLE: Lubricant-infused titanium surfaces with simultaneous anti-biofouling and targeted binding properties

AUTHOR: Yuxi Zhang, B.Eng. (Qingdao University of Science & Technology)

SUPERVISOR: Tohid F. Didar, Ph. D.

NUMBER OF PAGES: xiv, 78

## **Lay Abstract**

Biofouling is a major issue in implantable titanium devices such as coronary stents, plates and nails, and formation of biofilm on implants can lead to infection and failure of the device. Biofilms formed by bacterial adhesion could be resistant to antibiotics and can provoke a series of inflammatory response. Recent advances in anti-biofouling surface treatment has resulted in designing super slippery lubricant-infused omniphobic surfaces which are inspired from the *Nepenthes* pitcher plant. Liquid which is tethered on the surface offers a stable liquid interface, repelling both aqueous and organic liquids meanwhile showing excellent bacteria repellency. Lubricant-infused surfaces (LIS) are resistant towards biofilm formation and produce a stable surface that prevent non-specific adhesion. As a result of this repellent properties, LIS also repels the adhesion of desired biomolecules and cells such as osteoblasts, bone cells and growth factors which are essential factors for bone recovery at the implant-bone interface. Our motivation in this thesis is to create a lubricant-infused coating on titanium surfaces that possesses both bio-functional and blocking features. We designed surfaces that decrease implant infection caused by non-specific adhesion and simultaneously promote targeted binding of biomolecules and cells that will increase osseointegration of the implant to enable long-term fixation.

## **ABSTRACT**

Lubricant-infused surfaces (LIS) are created by modifying chemical and physical properties of surfaces with aim of lowering surfaces energy where designed surface will possess liquid-repelling behaviors under low tilting angles. LIS has great potential to be applied on implantable devices due to it is stable anti-biofouling properties under fluidic environment. However, a few studies have reported that the existing research on implant surface uses complicated methods and high cost fabrication to create LIS on titanium implants. Furthermore, current limitation of LIS coatings for titanium implants lies in the lack of tissue integration and cell interaction. As a result, LIS prevents both bacteria and bone cells from adhering to the interface between implant and natural bone. This unselective blocking is problematic for titanium implants used in orthopaedic surgery when devices are required to possess tissue integration properties to facilitate long term fixation in the human body. The overall objective of this thesis is to apply LIS on titanium surfaces via a chemical modification technique and simultaneously integrate bio-functional features onto LIS to promote osteoblasts adhesion. In this project, chitosan and collagen were used to facilitate cell adhesion. To start with, three methods were used to immobilize chitosan on titanium to obtain the desired bio-functional LIS coatings: (1) LIS on top of (3-Glycidyloxypropyl)trimethoxysilane (GPTMS) crosslinked chitosan; (2) LIS on dip-coated chitosan; (3) LIS generated from GPTMS and Trichloro(1H,1H,2H,2H-perfluorooctyl)silane (TPFS) mixed silanes modified titanium surface followed by chitosan functionalization. Among these modification techniques, method (3) showed optimal anti-biofouling and osseointegration properties. Since collagen is well known for increase of

cell interactions, it was used via mixed silanes functionalization method. Finally, the properties were compared with chitosan coated surfaces. During tests, surface wettability was measured, anti-biofouling properties and osseointegration was examined with staphylococcus aureus and SAOS-2 cells, respectively. We found that chitosan modified surfaces using method (3) not only significantly increased cell adhesion in comparison with the other two modification methods, but also dramatically decreased bacterial adhesion compared to collagen coated LIS on titanium. Although collagen has better cell adhesion properties than chitosan, collagen coated surface significantly decreased antibiofouling properties. In conclusion, bio-functional lubricant-infused titanium surfaces created by chemical vapor deposition (CVD) method with mixed silanes is a feasible and straightforward method to immobilize biomaterials and stabilize the lubricant layer on titanium substrates. Chitosan coated LIS on titanium prevents bacterial adhesion and simultaneously promotes targeted cell binding.

## **ACKNOWLEDGEMENTS**

I would like to thank Dr. Tohid F. Didar for giving me a chance to join his research group. Furthermore, Dr. Zeinab Hosseini-Doust gave me insightful advice in biofilm formation experiment and I had a very good cooperation with her student Claudia. In addition, I am also grateful to my colleagues, especially Maryam, Martin and Amid. Maryam build my basic knowledge in cell culture experiment and always answer my doubts both in research and campus life. Martin taught me fabrication of microfluidic chip and surface treatment skills. Furthermore, Amid is always approachable and willing to share knowledge with me. Last not least, I want to thank my family that they always have my back. I would like to say it is impossible for me to complete my project without their help and encouragement.

## TABLE OF CONTENT

Lay Abstract.....	iii
ABSTRACT.....	iv
ACKNOWLEDGEMENTS.....	vi
TABLE OF CONTENT.....	vii
LIST OF FIGURES.....	ix
LIST OF EQUATION.....	xii
LIST OF ABBREVIATIONS AND SYMBOLS.....	xiii
DECLARATION OF ACADEMIC ACHIEVEMENT.....	xv
CHAPTER ONE: INTRODUCTION AND OBJETIVES.....	1
1.1 Clinical issues of implantable titanium devices.....	1
1.2 Anti-bacterial surface coatings on titanium implants.....	2
1.2.1 Bactericidal surface coatings.....	3
1.2.2 Anti-biofouling surface coatings.....	4
1.3 Lubricant-infused surfaces (LIS) for biomedical implants.....	6
1.3 Research Objectives.....	8
CHAPTER TWO: BACKGROUND.....	9
2.1 Mechanism of action of LIS and current preparation methods.....	9
2.2 Bio-integration on titanium implants.....	14
2.2.1 Surface structuring and chemical modification.....	15
2.2.2 Bio-functional modification on titanium surface.....	15
2.2.3 Chitosan immobilization techniques.....	18
2.2.4 Collagen immobilization techniques.....	19
CHAPTER THREE: MATERIALS AND METHOD.....	21
3.1 Materials.....	21
3.2 Methods.....	22
3.2.1 Preparation of LIS on titanium substrates.....	22
3.2.2 Biofunctionalized lubricant-infused chitosan-GPTMS crosslinked coating.....	24
3.2.3 Biofunctionalized lubricant-infused DHB-chitosan conjugated layer-by-layer coating.....	26
3.2.4 Biofunctionalized lubricant-infused chitosan conjugated coating created using mixed silanes.....	28

3.2.5 Biofunctionalized lubricant-infused collagen conjugated coating created using mixed silanes .....	30
3.2.6 Contact and sliding angle measurement .....	32
3.2.7 Biofilm formation .....	33
3.2.8 Cell adhesion and biofunctionality of modified titanium surfaces .....	34
CHAPTER FOUR: RESULTS AND DISCUSSION .....	36
4.1 Surface Wettability .....	36
4.1.1 Wettability of lubricant-infused titanium surfaces.....	36
4.1.2 Wettability of chitosan coated titanium surfaces .....	38
4.1.3 Wettability of mixed silanes modified titanium surface .....	41
4.2 Anti-biofouling Properties .....	44
4.2.1 Bacteria repellency properties of LIS modified titanium substrate .....	44
4.2.2 Bacteria repellency of chitosan modified titanium surfaces .....	46
4.2.3 Bacteria repellency of mixed silane modified titanium surfaces .....	49
4.3 Cell adhesion experiments .....	53
4.3.1 Biofunctionalized lubricant-infused DHB-chitosan coated titanium surfaces..	53
4.3.2 Biofunctional lubricant-infused surfaces created using mixed silanes .....	57
CHAPTER FIVE: CONCLUSION.....	63
REFERENCE.....	65

## LIS OF FIGURES

Figure 1. Schematic representation of bacterial adhesion and proliferation on surfaces and the antibiotic resistance effect caused by biofilm formation. ....	2
Figure 2. Schematic representation of anti-biofouling properties of lubricant-infused surfaces (LIS).....	6
Figure 3. Schematic representation of a droplet on the lubricant-infused rough surface, A) droplet completely encapsulated by the lubricant; B) droplet lays on top of lubricant. ....	10
Figure 4. Schematic representation of preparing LIS on titanium substrates. ....	23
Figure 5. Schematic representation of creating biofunctionalized lubricant-infused chitosan-GPTMS crosslinked coating.....	25
Figure 6. Schematic representation of creating a layer-by-layer biofunctionalized lubricant-infused DHB-chitosan conjugated coating.....	27
Figure 7. Schematic representation of creating bio-functional lubricant-infused chitosan conjugated surfaces using mixed silanes. ....	29
Figure 8. Schematic representation of creating biofunctionalized lubricant-infused collagen conjugated coatings using mixed silanes.....	31
Figure 9. The contact angle and sliding angle measurements of water droplet on untreated titanium (Ti), and TPFS modified titanium samples (Ti-FS), A) static contact angle results of surfaces before adding lubricant layer, B) sliding angle results of the surfaces after adding the lubricant layer. Each group has three samples and each sample was measured for three times. Error bars represent the standard division (SD) of the mean of at least three samples. **P < 0.01 and ***P < 0.0001 compared with Ti control samples. ....	37
Figure 10 The contact angle and sliding measurements of water droplet on control and experimental groups, A) Static contact angle results of surfaces before adding lubricant layer, B) Sliding angle results of the surfaces after adding the lubricant layer. Each group has three samples and each sample was measured for three times.	

Error bars represent the SD of the mean of at least three samples. \*\*\*  $P < 0.001$  and \*\*\*\*  $P < 0.0001$  when compared with chitosan-GPTMS and chitosan-DHB respectively. ....40

Figure 11. The contact angle and sliding measurements of water droplet on control and experimental groups, A) static contact angle results of surfaces before adding lubricant layer, B) sliding angle results of the surfaces after adding the lubricant layer. Each group has three samples and each sample was measured for three times. Error bars represent the SD of the mean of at least three samples. \*\*\*\*  $P < 0.0001$  when compared with control samples. ....43

Figure 12. Results obtained from the bacterial adhesion studies on uncoated and coated Ti substrates using crystal violet staining assay. Ti-FS+L surfaces significantly prevented bacterial adhesion and biofilm formation when compared to untreated Ti and Ti-FS surfaces. Whiskers span the first quartile and fourth quartile range of at least 3 samples. \*\*  $P < 0.01$  when compared with Ti-FS+L samples. ....45

Figure 13. Crystal violet staining assay for investigating the antifouling properties of the modified surfaces, A) detachment of membrane observed on chitosan-GPTMS and chitosan-GPTMS-FS+L groups, B) Stability of chitosan-DHB and chitosan-DHB-FS+L samples after biofilm experiment. ....47

Figure 14. Crystal violet evaluation of *S. aureus* biofilm formation on control and experimental groups. Whiskers span the first quartile and fourth quartile range of at least 3 samples. \*\*  $P < 0.01$  and \*  $P < 0.05$  when compared with Ti and chitosan-DHB groups, respectively. ....48

Figure 15. Crystal violet evaluation of *S. aureus* biofilm formation on control groups and experimental groups. Whiskers span the first quartile and fourth quartile range of at least 3 samples. \*\*\*\*  $P < 0.0001$ , \*\*  $P < 0.01$  and \*  $P < 0.05$  when compared with Ti and GPTMS75-TPFS25-chitosan+L group, respectively. ....52

Figure 16. SaOS-2 cell proliferation after 3 days visualized by fluorescence spectroscopy (nuclei: blue; microfilaments: red) on the surface of control and experimental groups, A) Representative fluorescence images showing the density and distribution

of adherent cells, B) statistical analysis of cell attachment and proliferation on different samples. Error bars represent the SD of the mean of at least three samples. \*\* P < 0.01 and \* P < 0.05 when compared with Ti-FS+L samples. ....55

Figure 17. Immunofluorescence staining of cell nucleus and actin-based cytoskeleton (nuclei: blue; microfilaments: red) in human SAOS-2 cells to observe cell morphology and spreading.....56

Figure 18. SaOS-2 cell proliferation after 3 SaOS-2 cell proliferation after 3 days visualized by fluorescence microscopy (nuclei: blue; microfilaments: red) on the surface of control and experimental groups, A) Representative fluorescence images showing the density and distribution of adherent cells, B) Number of adherent cells on control and treated titanium after 3of cell culture. Error bars represent the SD of the mean of at least three samples. \*\*\* P < 0.001, \*\* P < 0.01 and \* P < 0.05 when compared with control samples. ....59

Figure 19. SaOS-2 cell proliferation after 7 days visualized by fluorescence microscopy (nuclei: blue; microfilaments: red) on the surface of control and experimental groups, A) Representative fluorescence images showing the density and distribution of adherent cells, B) Number of adherent cells on control and treated titanium after 3 and 7 days of cell culture. Error bars represent the SD of the mean of at least three samples. \*\*\* P < 0.001 and \*\* P < 0.01 when compared with control samples. ....60

Figure 20. Immunofluorescence staining of nucleus and actin-based cytoskeleton (nuclei: blue; microfilaments: red) in human SAOS-2 cells to observe cell morphology after 7 days of cell culture. ....62

## LIST OF EQUATION

Equation 1 $S_{os(a)} < -\gamma_{oa} \left( \frac{r-1}{r-\phi} \right)$ .....	11
Equation 2 $S_{os(a)} = \gamma_{sa} - \gamma_{os} - \gamma_{oa}$ .....	11
Equation 3 $S_{os(w)} = \gamma_{sw} - \gamma_{os} - \gamma_{ow}$ .....	11
Equation 4 $S_{os(a)} < -\gamma_{oa} \left( \frac{r-1}{r-\phi} \right)$ .....	12
Equation 5 $-\gamma_{oa} \left( \frac{r-1}{r-\phi} \right) < S_{os(a)} < 0$ .....	12
Equation 6 $S_{os(a)} \geq 0$ .....	12
Equation 7 $S_{os(a)} \geq 0$ .....	12
Equation 8 $-\frac{\gamma_{ow}(r-1)}{r-\phi} < S_{os(w)} < 0$ .....	12

## LIST OF ABBREVIATIONS AND SYMBOLS

$\mu\text{m}$	micrometer
$\text{mm}$	millimeter
$^{\circ}\text{C}$	degree Celsius
$\text{mg}$	milligram
$\text{min}$	minute
$\text{s}$	second
$\%$	per cent
<b>SLIS</b>	slippery liquid infused surface
<b>LIS</b>	lubricant-infused surface
<b>LPD</b>	liquid phase deposition
<b>CVD</b>	chemical vapor deposition
<b>TPFS</b>	trichloro(1H,1H,2H,2H-perfluorooctyl) silane
<b>PFPP</b>	perfluoroperhydrophenanthrene
<b>DI</b>	deionized water
<b>S. aureus</b>	staphylococcus aureus
<b>LB</b>	lysogeny broth
<b>CV</b>	crystal violet
<b>GAGs</b>	glycosaminoglycans
<b>GPTMS</b>	(3-Glycidyloxypropyl)trimethoxysilane

<b>APTES</b>	(3-Aminopropyl)triethoxysilane
<b>BSA</b>	bovine serum albumin
<b>PBS</b>	phosphate-buffered saline
<b>FBS</b>	fetal bovine serum
<b>DAPI</b>	(4',6-diamidino-2-phenylindole)
<b>EDC</b>	1-ethyl-3-(3-dimethylaminopropyl)carbodiimide
<b>NHS</b>	N-hydroxysuccinimide
<b>LB</b>	Luria-Bertani medium
<b>TSB</b>	tryptic soy broth
<b>TSBC5</b>	TSB with 0.5% glucose, 0.2% sodium citrate, 0.6% yeast extract
<b>SEM</b>	scanning electron microscopy

## **DECLARATION OF ACADEMIC ACHIEVEMENT**

I, Yuxi Zhang, performed wettability measurement, analysis of water contact angle and sliding angle, roughness and topography measurements, cell culture experiments, analysis of biofilm formation data, statistical analyses and wrote the thesis. Dr. Tohid Didar supervised my project. Dr. Tohid Didar and Dr. Maryam Badv provided guidance on testing and analysis and editorial suggestions during writing of my thesis. Experiments of bacteria cultivation was performed by Claudia Alonso Can.

## **CHAPTER ONE: INTRODUCTION AND OBJETIVES**

### **1.1 Clinical issues of implantable titanium devices**

Due to high modulus and strength,<sup>1</sup> biocompatibility,<sup>2</sup> high resistance to degradation, wear and fatigue,<sup>3</sup> titanium is widely used in biomedical implants. However, there are several clinical complications related to titanium medical devices. Currently, implant failure caused by biofilm formation and infection is a prevalent and significant clinical issue which increases the implant associated mortality and morbidity rates and adds a financial burden on the healthcare system. For example, estimated cost of an infected prosthetic joint replacement in the U.S. is around \$50,000 to \$60,000.<sup>4</sup> Biofilm is formed by bacteria attachment, proliferation and spreading (**Figure 1**) on the implant surface and it is reported that approximately 14% of total implant failures are caused by biofilm formation.<sup>5</sup> According to the report from the Canadian Joint Replacement Registry (CJRR), approximately 130,000 hip and knee replacement operated in Canada between 2017 and 2018. Among them, hip replacements accounted for 58,492 and knee replacements was 70,502. But more than 9,700 hip and knee replacement revision surgeries were performed in 2017-2018, hip and knee replacement revisions represent 8.2% and 6.9% of total number of their initial replacements. Furthermore, 17.7% of the total revisions was caused by infection issue.<sup>6</sup> The sources of infectious bacteria can from environment such as the surgery room, equipment, the resident bacteria on patient's skin or the bacteria already inside human's body.<sup>7</sup> Most biofilms formed by bacterial adhesion are resistant towards antibiotics that result in bacterial antibiotic resistance, creating a global issue.<sup>8</sup>

To solve the clinical complications associated with infection and biofilm formation on implants, different surface modification approaches have been implemented. These strategies involve creating bactericidal surface coatings with polycations,<sup>9</sup> antimicrobial peptides<sup>10</sup> and antibiotics<sup>11</sup> and anti-biofouling coatings such as microstructure fabrication,<sup>12</sup> hydrophilic chains incorporation,<sup>13</sup> polymer brush coatings<sup>14</sup> and lubricant-infused coatings<sup>15</sup>. Categories, pros and cons of these surface coating strategies will be discussed in the following sections.

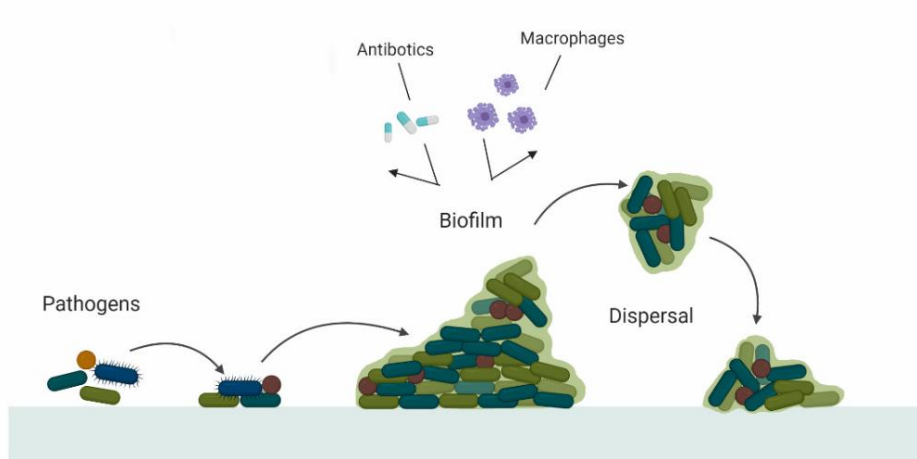


**Figure 1.** Schematic representation of bacterial adhesion and proliferation on surfaces and the antibiotic resistance effect caused by biofilm formation.

## 1.2 Anti-bacterial surface coatings on titanium implants

Anti-bacterial coatings can be divided into bactericidal and anti-biofouling coatings based on the interaction between the bacteria and implant surface. To be more specific, bactericidal surfaces disrupts bacteria at cellular level and cause bacteria cell death. In

contrast, anti-biofouling coatings resist bacteria adhesion by offering bacterial repellent topography or chemical properties.<sup>16</sup>

### **1.2.1 Bactericidal surface coatings**

Bactericidal surfaces are usually obtained by surface functionalization with antibiotics,<sup>17</sup> polymeric material<sup>18</sup> or nano particles<sup>19</sup>. Some surface functionalization techniques use physical strategies which create thin films via hydrogen or electrostatic interaction,<sup>20</sup> physical entrapment or self-assembly<sup>21</sup> to incorporate biomolecule or hydrophilic polymers, disrupting bacteria at cellular level. Although these surface coating strategies have exhibited promising antibacterial properties, the stability of the coating is an issue.

In contrast to physical modification techniques, chemical modification strategies firstly create active surfaces with functional groups and pave the foundation for binding with bactericidal molecules in following steps. Pre-activations techniques such as oxidation<sup>22</sup> and aminolysis<sup>23</sup> are used to provide active amine groups<sup>24</sup> and hydroxyl groups as anchors during surface grafting reactions. After modification, surfaces are bounded with biocide molecules, materials or medicine, such as metallic nano particles,<sup>11</sup> polycations,<sup>9</sup> antimicrobial peptides<sup>10</sup> and antibiotics<sup>11</sup> to interfere bacterial adhesion, proliferation and growth.

Although antibiotic bactericidal surface is a widely used coating method, they still have some limitations. First of all, many results demonstrate that all antibiotics, either used alone or combined with other materials, are released with an initial burst and their antimicrobial activity is dose-dependent.<sup>25</sup> Additionally, antibiotic resistance on the medical implants is another factor that reduces bactericidal efficiency of coatings.<sup>26</sup> To circumvent these

limitations, current strategies of development have shifted towards using other molecules instead of antibiotic drugs in bactericidal surface coatings.

Among bactericidal molecules, chitosan is a natural biodegradable biomaterial with non-toxic degradation products<sup>27</sup> and has a broad-spectrum of antibacterial activity on bacteria, including *Escherichia coli*, *Staphylococcus aureus*, *Bacillus subtilis* and *Actinomyces naeshlundii*.<sup>28</sup> In recent years, Gomes *et. al* reported a layer-by-layer (LBL) assembled chitosan/alginate coating and showed that this surface coating decreases the growth of bacteria by 65–80%.<sup>29</sup>

It is also claimed that chitosan induces proliferation of osteoblast cells, mesenchymal cells and neovascularization *in vivo*.<sup>30</sup> Antonia G. Moutzouri group demonstrated that chitosan coated glass surfaces have higher elastic modulus of attached osteoblasts compared to uncoated control surfaces. This conclusion was further confirmed in the research by Simon *et al.*, showing that elastic moduli of adherent cells on chitosan coated surfaces is between 8 and 400 KPa by AFM (atomic force microscope).<sup>31</sup> Additionally, cells were more stable on chitosan coated surfaces and the detachment strength of osteoblasts on chitosan coating was increased within the first hour of cell culture measured by micropipette aspiration technique.<sup>31</sup>

### **1.2.2 Anti-biofouling surface coatings**

Anti-biofouling coatings alter physical properties of the surface by changing wettability, surface energy and surface topography. Physical properties of substrates can be modified by different techniques such as microstructure fabrication,<sup>12</sup> hydrophilic chains

incorporation,<sup>13</sup> polymer brush coatings,<sup>14</sup> lithography,<sup>32</sup> plasma etching,<sup>33</sup> hydrothermal synthesis,<sup>34</sup> micro-moulding, laser interference patterning<sup>35</sup> and anodization.<sup>36</sup>

In recent years, attention has been drawn towards biomimetic anti-biofouling surfaces where surface construction is inspired from nature, such as gecko foot,<sup>37</sup> insect wings<sup>38</sup> and plant leaves.<sup>39</sup> Among them, lubricant-infused surfaces (LIS) inspired by nepenthes pitcher plants with omniphobic characteristics have gained extensive attention. A slippery liquid-infused surface is created by infiltration of the micro structures present on the surface in moist environment (**Fig. 2**), so that insects cannot adhere on to the surface and slip into stomach of pitcher plants.<sup>40</sup> Furthermore, LIS has advantages over lotus leaves inspired hydrophobic coatings from following aspects:

As for superhydrophobic surfaces, damage on the surface will decrease anti-biofouling robustness. Additionally, trapped air pockets may collapse under low surface tension liquid, making surfaces lose their hydrophobicity. Nevertheless, bacteria repellency of LIS has better stability in liquid or fluidic environment, making it preferable in implantable application.<sup>41</sup>

LIS coatings can play an important role in creating anti-fouling surfaces for medical implants because they can be integrated into many types of material, including metals such as stainless steel<sup>42</sup> and titanium<sup>43</sup>. Recently, approaches of LIS are reported to have high bacteria resistance and anti-clotting function.<sup>44</sup> Epstein *et al.* demonstrated LIS reduced biofilm coverage of *Staphylococcus aureus* by 97% in their most recent study.<sup>45</sup> In an

earlier study, Badv *et al.* reported omniphobic lubricant-infused catheters significantly attenuated clot formation compared with uncoated surfaces.<sup>45</sup>

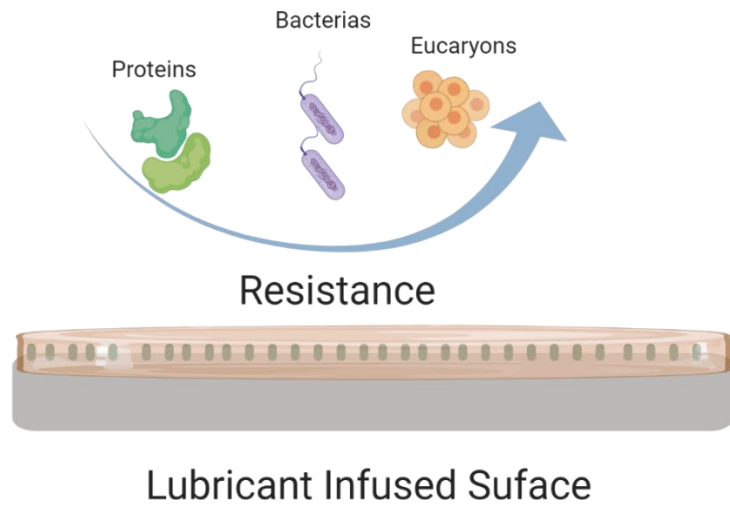


**Figure 2.** Schematic representation of anti-biofouling properties of lubricant-infused surfaces (LIS).

### **c1.3 Lubricant-infused surfaces (LIS) for biomedical implants**

LIS are produced by modifying chemical and/or physical properties of the surface and further infiltrating the surface with an appropriate lubricant layer that possesses high affinity towards the underlying solid substrate.<sup>46</sup> Surface topography and chemical features are two key factors for adjusting surface property to match the chemistry of lubricant,<sup>47</sup> involving electrospinning,<sup>48</sup> electrochemical deposition,<sup>49</sup> nanopillar assembly,<sup>50</sup> polymer wrinkling,<sup>51</sup> chemical and physical etching<sup>52</sup> by altering surface topography.

On the other hand, chemical modification is another method applied on surface to offer a higher affinity to lubricant layer. Liquid-phase deposition (LPD) and chemical vapor deposition (CVD) are the two common chemical modification techniques used to create LIS. Recently, CVD has shown to create more uniform coatings and be less harmful for the substrate compared with LPD methods.<sup>44</sup> During LPD process, self-polymerization of silanes in the solution impairs homogeneity of silane layer and harmful solvent waste produced during the procedure limits industrial viability of the process.<sup>53-55</sup>

Although various kinds of LIS have been revealed with outstanding features for bacterial resistance, the coating still has some limitations when applied on metal alloys. Doll *et al.* reported a method that uses ultrashort pulse laser ablation to fabricate nano structure on titanium surfaces. Fabricated samples were dip coated with a fluorinated polymer to avoid oil creeping on surface, followed by forming a homogeneous liquid film with perfluoropolyether lubricant (Krytox GPL) by spin coating on surface. Lubricant infiltrated samples exhibited high bacteria resistance properties.<sup>43</sup> However, laser micromachining is reported to form heat affected zones and cause material property alteration and thermal stress<sup>56</sup> In addition, an extra step is required to remove machining debris from molten material and recast layer. Furthermore, precision of ultra fast machining is influenced by deformation of laser in focal plane.<sup>56</sup>

In addition to preventing bacterial adhesion, a strong and durable bone-implant connection is required for titanium implants used in some surgeries such as bone anchored limb prosthesis and knee and joint replacement.<sup>57</sup> Current techniques of LIS on titanium still

lack bioactivity and they simultaneously block osteoblasts and bacteria adhesion, indistinctively.<sup>43</sup>

### **1.3 Research Objectives**

Based on the current developments of LIS in preventing non-specific adhesion, the focus and objective of this thesis was to develop bio-functional LIS on titanium implants with high osteoblast affinity. This thesis focuses on developing bio-functional LIS coatings for titanium surfaces where osteoblast attachment and proliferation are enhanced, without compromising the blocking and antifouling properties of the lubricant-infused layer.

CVD method is used in our project to prepare LIS on titanium implants through 3 methodologies: (1) LIS integrated into the GPTMS crosslinked chitosan; (2) LIS integrated into the dip-coated catechol conjugated chitosan and 3) LIS generated from GPTMS and TPFS mixed silanes modified titanium surface, followed by chitosan functionalization. Afterwards, collagen as an alternative biomaterial with enhanced bioactivity was used and the results were compared with chitosan coated surfaces in both biofilm and cell culture experiments. Finally, the optimized method for achieving bioactive LIS anti-biofouling titanium implants is reported.

## CHAPTER TWO: BACKGROUND

### 2.1 Mechanism of action of LIS and current preparation methods

Inspired by the *Nepenthes* pitcher plant, LIS show excellent repellency properties towards organic and aqueous fluids.<sup>58</sup> Nectar and water can be locked into the microscale structures present on the pitcher plant and produce a stable yet dynamic layer of lubricant where the friction between insects' feet and film is pretty low and non-specific adhesion is prevented. Wong, T. S. *et al.* made a slippery lubricant-infused surface to repel both organic and aqueous solutions where only a slight tilting angle could make the droplets slide off the surface.<sup>55</sup> **Fig. 3** illustrates a model of this lubricant-infused slippery surface.

To design LIS, three main design criteria must be met: (1) The lubricant and droplet liquid must be immiscible, (2) the lubricant oil phase must wet and spread on substrate, and (3) the solid substrate should have a higher affinity to lubricant over the contaminating droplet liquid.<sup>59</sup> Furthermore, air phase, lubricant oil phase, solid substrate and droplet liquid phase are four phases involved in a LIS system. Interactions among the four phases determine morphology of contact line and mobility of the droplet on surface.<sup>60</sup>

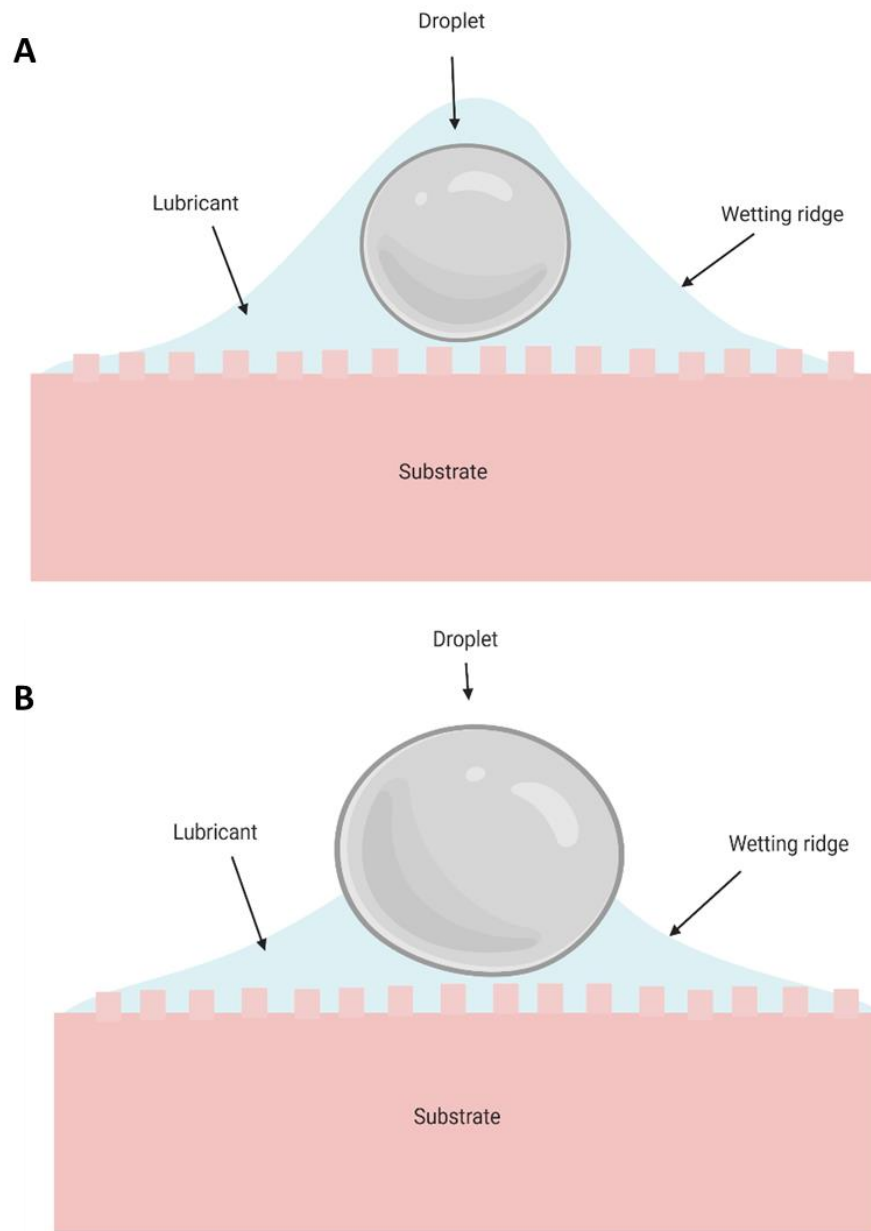


**Figure 3.** Schematic representation of a droplet on the lubricant-infused rough surface, **A**) droplet completely encapsulated by the lubricant; **B**) droplet lays on top of lubricant.

$S_{ow(a)}$  is defined as the spreading coefficient of water droplet on lubricant oil phase in an air environment.

$$S_{ow(a)} = \gamma_{wa} - \gamma_{ow} - \gamma_{oa} \quad \text{Equation 1}$$

When  $S_{ow(a)} > 0$ , droplet will be completely encapsulated by the lubricant (**Fig. 3A**).

If  $S_{ow(a)} < 0$  droplet will lay on top of lubricant, as it showed in **Fig. 3B**. In equation (1),  $\gamma_{wa}$  represents water-air surface tension,  $\gamma_{ow}$  is oil-water surface tension, and  $\gamma_{oa}$  stands for oil-air surface tension.

In equation (2) and (3),  $S_{os(a)}$  is spreading coefficient of oil on a solid surface in contact with air, and  $S_{os(w)}$  stands for spreading coefficient of oil on a solid surface that is in contact with water.  $\gamma_{sw}$ ,  $\gamma_{sa}$  and  $\gamma_{os}$  represent surface tension at solid-water, solid-air and oil-solid interfaces, respectively.

$$S_{os(a)} = \gamma_{sa} - \gamma_{os} - \gamma_{oa} \quad \text{Equation 2}$$

The lubricant has a higher affinity to the substrate over the water droplet, if  $S_{os(w)} \geq 0$ .<sup>47</sup>

$$S_{os(w)} = \gamma_{sw} - \gamma_{os} - \gamma_{ow} \quad \text{Equation 3}$$

Young's relation and Cassie–Baxter to Wenzel transition is used to explain how trapped air pockets on rough surfaces offer hydrophobicity to the substrate.<sup>61</sup> On LIS, the lubricant oil phase has higher affinity to wet the solid substrate than the contaminating droplet liquid. Thus, air phase trapped in surface is replaced by lubricant. Criteria of this system is defined by substrate roughness and surface tensions which are concluded by J. David Smith *et al.*:<sup>61</sup>

Model 1: Lubricant does not wet substrate:

$$S_{os(a)} < -\gamma_{oa} \left( \frac{r-1}{r-\phi} \right) \quad \text{Equation 4}$$

Model 2: Lubricant partially wets the surface:

$$-\gamma_{oa} \left( \frac{r-1}{r-\phi} \right) < S_{os(a)} < 0 \quad \text{Equation 5}$$

Model 3: Lubricant completely wets the surface:

$$S_{os(a)} \geq 0 \quad \text{Equation 6}$$

Requirement for higher affinity for lubricant over droplet on substrate surface:

$$S_{os(a)} \geq 0 \quad \text{Equation 7}$$

$$-\frac{\gamma_{ow}(r-1)}{r-\phi} < S_{os(w)} < 0 \quad \text{Equation 8}$$

When configuration meet LIS requirement, lubricant completely spreads on the substrate and repels the contaminating droplet off with a wetting ridge as it is illustrated in **Fig. 3B**.<sup>62</sup>

$\phi$  is the fraction of projected area occupied by the droplet liquid and  $\gamma$  is only a function of texture parameters and won't be affected by surrounding environmental factors. Given that surface wettability is mainly influenced by surface tension, tuning surface chemical properties and surface roughness are feasible ways to build LIS.<sup>63</sup>

LIS repels both high surface tension aqueous and low surface tension organic liquids, for examples water (72.3 mN/m) and hexadecane (27.5 mN/m). This omniphobic function of LIS plays an important role in the anti-biofouling properties on implantable surfaces.<sup>60</sup>

The underlying substrate and the wetting lubricant work together to maintain a dynamic but stable oil layer on flat or rough surfaces. Most importantly, the surface must have a chemistry that matches the chemical nature of the infusing oil phase. Thus, different methodologies have been purposed to modify surface roughness and chemical features of surface to achieve functional and repellent LIS.<sup>64</sup>

As it mentioned above, the solid substrate could be textured to help lubricant retention. Early methods to obtain slippery surfaces involved using photolithography on a photoresist coated surface and casting PDMS on pitcher plant's peristome.<sup>65</sup> Other methods to create nanostructures on substrate include soft lithography,<sup>66</sup> etching,<sup>67</sup> emulsion and phase separation,<sup>68</sup> mold transcribing,<sup>65</sup> electrospinning,<sup>69</sup> electrochemical deposition,<sup>70</sup> nano particle assembly,<sup>71</sup> polymer-induced wrinkling<sup>71</sup> and layer-by-layer manufacturing.<sup>72</sup>

LIS could also be achieved by changing the surface chemical properties of the substrate. A proper chemical layer is applied on surface to induce low surface energy that has higher affinity towards the lubricant layer. Chemical modification techniques include liquid-phase deposition (LPD), dip-coating, spray-coating, and chemical vapor deposition (CVD).<sup>73</sup> Compared with LPD, CVD is preferable as it creates more uniform coating especially on nonplanar surfaces or even geometrical shapes. Meanwhile, compared to LPD, fewer chemical reactants are used in the CVD process making this technique a more eco-friendly modification method.<sup>74</sup> Additionally, solid substrates may be eroded during the LPD process by being exposed to corrosive by products produced during the LPD method, an effect that can be alleviated through CVD method.<sup>73</sup>

In the final step, a compatible lubricant is added to the solid surface to create a layer of oil phase through capillary wicking on rough surface or van der Waals force on chemically modified surfaces.<sup>75</sup> The lubricant layer has shown to remain stable under flow conditions and when placed in closed environments.<sup>55</sup>

## **2.2 Bio-integration on titanium implants**

The ability of titanium implants to connect with the host bone is a fundamental requirement for long-term orthopedic implants. The functional connection between the bone and the loading-bearing implant surface is defined as osseointegration.<sup>76</sup> Formation of fibrous tissues and loosening of prostheses are symptoms of insufficient osseointegration.<sup>77</sup> When implants lack surface interaction with the bone, there is a good chance that inflammation with fibrous aseptic loosening will happen and implant will be rejected.<sup>78</sup> Given that osseointegration is a prerequisite for orthopedic implants, regeneration and remodelling of bone tissue around implant is an important index to measure bio-integration of implant. Hence, surface modifications are applied on titanium implant surfaces to regenerate and remodel bone tissue on implants.<sup>79</sup>

Osteoblasts and osteoclasts maintain dynamic metabolic balance of bone tissue where osteoclasts break down the bone to free the calcium. Osteoblasts deposit calcium into bone and remodel it.<sup>80</sup> Among them, osteoblasts are derived from mesenchymal stem cells and are responsible for bone matrix synthesis and mineralization which are essential to the healing of bone.<sup>81</sup> In order to attract osteoblasts and functionalize the implant for bio-integration, the chemical and physical properties of the surface are altered through chemical

modification and surface structuring techniques.<sup>82</sup> These modification methods are discussed in the further sections.

### **2.2.1 Surface structuring and chemical modification**

Surface roughness, wettability and chemistry affect cell attachment on implants. As moderately roughen implant surface can enhance recruitment of osteoblasts to surface and stimulates osteogenic maturation, several chemical and physical methods are used to enhance the nanotopography on the implant surface.<sup>83</sup> Korotin *et al.* showed that treatment of titanium surface with hydrofluoric acid increased surface energy and bio-acceptability of the implant, characterized by X-ray photoelectron spectroscopy (XPS).<sup>84</sup> In another study, titanium implants were blasted with titanium oxide particles and showed advanced contact between bone and metal in histomorphometry analysis after being inserted in maxilla and mandible.<sup>85</sup> Sand-blasted, acid-etched titanium surfaces and titanium surfaces treated with sodium bicarbonate solution also showed increased roughness,<sup>86</sup> and hydroxyl groups on surface are proved to present advantages in initial stages of osseointegration and facilitating bone integration.<sup>87</sup> In addition to above technologies, laser treatment,<sup>88</sup> electropolishing,<sup>89</sup> pulsing technique<sup>90</sup> and micro-arc oxidation<sup>91</sup> also exhibited improvement in biocompatibility of implants.

### **2.2.2 Bio-functional modification on titanium surface**

Immobilization of biomolecules on implant surfaces is a promising strategy for creating a bioactive titanium surface.<sup>92</sup> The biomolecules used to create a bio-functional bone implant

must support the adhesion, organization, differentiation and mineralization of osteoblasts and osteoprogenitor cells.<sup>92</sup>

Owing to good hemostatic properties and negligible cytotoxicity, collagen is one of the most commonly used biomolecules for implant surface biofunctionalization.<sup>93</sup> Type I collagen is largely produced by osteoblasts in bone which is composed of an organic collagen matrix.<sup>92</sup> Collagen is immobilized on titanium by the reaction between hydroxyl and amino functional groups and the product showed no cytotoxic effects in lactate dehydrogenase-based assay. Higher degree of cell colonization was observed on collagen coated titanium substrates compared with uncoated titanium and spindle-shaped cytomorphology of osteoblasts was observed on coated samples *via* fluorescence microscopy.<sup>94</sup>

Additionally, growth factors such as bone morphogenetic proteins,<sup>95</sup> transforming growth factor- $\beta$ 1,<sup>96</sup> platelet-derived growth factor,<sup>97</sup> insulin-like growth factor<sup>98</sup> and fibroblast growth factor-fibronectin<sup>99</sup> are reported to be used for targeting cellular proliferation and differentiation.<sup>100</sup>

Bio-functional surfaces should increase osteoblasts adhesion and proliferation to help bone regeneration on surface. However, implants modified by growth factors also affect bone resorption process. For example, bone morphogenetic proteins are revealed to stimulate bone resorptive function of osteoclasts which negatively affects the desirable bone regeneration of osteoblast on implant surfaces.<sup>101</sup> Moreover, lack of stability limits

polypeptide applications on implants. In addition, pathogens may be transferred from animal to human body *via* extracted proteins, causing infections.<sup>102</sup>

DNA molecules possess distinctive advantages to growth factors. DNA molecules can transit to cell nucleus and help expression and production of specific mRNAs and proteins during the first one or two weeks of treatment.<sup>103</sup> Van den Beucken *et al.* illustrated that polyanionic salmon DNA coating improved mineralization of osteoblasts-like cells.<sup>104</sup> In another study, multilayered DNA (sterilized salmon testis DNA) and protamine coating provided a significantly higher bone-to-implant contact ratio during 3 weeks after implantation and promoted initial bone healing process.<sup>105</sup> Despite the exiting results obtained from DNA modified surfaces, current studies are relatively limited and need more animal experiments to prove DNA bioactivity on implant surfaces.<sup>92</sup>

Chitosan has been used in bone tissue engineering for over two decades, promoting cell adhesion, proliferation, and differentiation.<sup>106</sup> Chitosan as a natural polysaccharide can create a bed for osteoblasts ingrowth.<sup>107</sup> Additionally, osteoconductive and antimicrobial properties of chitosan make it a promising candidate for surface modification of titanium implants.<sup>108</sup> Moreover, the cationic nature of chitosan offers a suitable substrate for cell adhesion. Chitosan stimulates progenitor cells migration, enhances angiogenesis and accelerates extracellular tissue matrix reformation.<sup>109</sup>

Joel D. Bumgardner *et al.* reported that the attachment and growth of cells on chitosan coated titanium surface are contributed by the cationic nature of chitosan amine groups in cell culture test.<sup>108</sup> In another study, chitosan was grafted on titanium with 4-

(Triethoxysilyl)butanal silane and chitosan coated titanium surfaces showed supportive osteoblasts attachment and growth, confirmed with confocal microscopic analysis. Additionally, chitosan modified surfaces also induced 60% inhibition of gram-negative bacterial strain (*P. gingivalis* and *A. Naeslundii*) growth in only a few hours.<sup>110</sup>

### **2.2.3 Chitosan immobilization techniques**

Biomaterial-associated infections take a small percentage but serious complication in orthopaedic field.<sup>111</sup> Chitosan has good antibacterial properties against different bacteria, including *Escherichia coli*, *Staphylococcus aureus*, *Bacillus subtilis* and *Actinomyces naeslundii*.<sup>28</sup> The amino groups on chitosan possess a polycationic structure that react with anionic lipopolysaccharides of negative membrane surface.<sup>112</sup> Chitosan can kill bacteria by disrupting the bacteria membrane and destroys the bacteria barrier through polycationic binding.<sup>113</sup> In this process, positive charged amino groups on glucosamine monomer will interact with negatively charged microbial membrane, leading to intracellular constituents leaking.<sup>113</sup>

Modification methods to immobilize chitosan on titanium surfaces include alkyloxysilane deposition,<sup>107</sup> electrodeposition,<sup>114</sup> dip-coating, spin-coating,<sup>115</sup> physical vapor deposition (PVD)<sup>116</sup> and layer-by-layer self-assembly<sup>117</sup>.

Among them, chitosan- $\gamma$ -glycidoxypropyltrimethoxysilane (GPTMS), a type of chitosan-siloxane hybrid membrane, is reported to be biocompatible with human osteoblasts and bone marrow cells.<sup>118</sup> Further studies show that the conjugation of chitosan and catechol molecules *via* Schiff base reaction (reaction between amine group on chitosan and aldehyde

group on catechol with acetic acid catalyst) on titanium implants has long-lasting muco-adhesive properties.<sup>119</sup>

#### **2.2.4 Collagen immobilization techniques**

Type I collagen, as vertebrates' richest protein, can stimulate and accelerate osteogenic differentiation and mineralization of marrow stromal cells.<sup>120, 121</sup> Type I collagen is usually immobilized by immersing the desired surface in a collagen solution.<sup>122</sup> Titanium disks incubated with collagen type I solution for 15 min and rinsed with distilled water showed promoted osteoblast spreading and accelerated cellular extension, characterized by scanning electron microscopy (SEM).<sup>123</sup>

Other linking methods used for collagen grafting and deposition of titanium surfaces include polydopamine,<sup>124</sup> glutaraldehyde<sup>125</sup> and electrodeposition<sup>126</sup>. Collagen immobilized on polydopamine coated titanium surface showed better coating stability and cell adhesion compared with physical adsorption methods.<sup>124</sup> In the study from Shibata *et al.*, titanium disks grafted with type I collagen using glutaraldehyde as a crosslinking agent enhanced osteoblast differentiation and the extracellular fibers of osteoblasts suggested to be the primary mineralization sites that proved collagen promotes bone mineral deposition.<sup>125</sup> In electrodeposition methods, collagen molecules were attracted and immobilized on titanium electrodes under a charging potential where hydrophilic amino acids residues bonded to reactive hydroxyl functional group on titanium electrodes.<sup>127</sup>

In addition to these methods, organosilanes play an important role in binding organic and inorganic materials through hydrolysis and condensation of alkoxy groups.<sup>128</sup> 3-

aminopropyltriethoxy (APTES) is a coupling agent used for biomolecule immobilization and grafting on different materials.<sup>129</sup> In a study reported by Sharan *et al.* APTES was used to bind collagen to alkali treated titanium . The coupling reaction occurs between carboxyl groups on collagen and amino groups on APTES with 1-ethyl-3-(3-dimethyl aminopropyl) carbodiimide (EDC) and N-hydroxysuccinimide (NHS) activation.<sup>130</sup> It also revealed that cells were much smaller and showed a round shape on collagen-free surface but exhibited better cell spreading and well-organised cytoskeletons on APTES-collagen modified titanium dental implants.<sup>131</sup>

## **CHAPTER THREE: MATERIALS AND METHOD**

### **3.1 Materials**

Titanium (Grade 5, Ti<sub>6</sub>Al<sub>4</sub>V) sheets (1.6 mm x 30.5 cm x 30.5 cm) were purchased from McMaster-CARR, Canada and cut into 7 mm diameter discs through Water jet cutting by CIM Metals, Canada. Trichloro(1H,1H,2H,2H-perfluorooctyl) silane (TPFS) 97%, perfluoroperhydrophenanthrene (PFPP), (3-Glycidyloxypropyl)trimethoxysilane (GPTMS) 98% 100 ml, (3-Aminopropyl)triethoxysilane (APTES) 98%, Triton™ X-100 Surfact-Amps™ Detergent Solution 10 ml, phosphate-buffered saline (PBS), bovine serum albumin (BSA) 5 g, penicillin/streptomycin, 3,4-Dihydroxybenzaldehyde (DHB) 5 g, medium molecular weight chitosan 50 g and fetal bovine serum (FBS) were purchased from Sigma-Aldrich (Oakville, Canada). McCoy's 5A modified medium, Trypsin-EDTA (0.25%) and methanol-free formaldehyde, collagen I rat tail protein and DAPI (4',6-diamidino-2-phenylindole) were purchased from Thermo Fisher Scientific (Waltham, MA, USA). Phalloidin FITC Reagent was purchased from Abcam.

## **3.2 Methods**

In this project, titanium surfaces were treated with different modification procedures, to obtain biofunctionalized lubricant-infused titanium samples. Titanium substrates modified with LIS with no bio-functionality were tested as the control group. These modification procedures consisted of:

- 1) Lubricant-infused titanium surfaces (Ti-FS+L).
- 2) Biofunctionalized lubricant-infused chitosan-GPTMS crosslinked coating (chitosan-GPTMS-FS+L).
- 3) Layer-by-layer biofunctionalized lubricant-infused chitosan-DHB conjugated coating (chitosan-DHB-FS+L).
- 4) Biofunctionalized lubricant-infused chitosan coating created using mixed silanes (GPTMS75-TPFS25-chitosan+L).
- 5) Biofunctionalized lubricant-infused collagen coating created using mixed silanes (APTES75-TPFS25-collagen+L).

The methods to create each type of surfaces are explained in detail in the following sections.

### **3.2.1 Preparation of LIS on titanium substrates**

Titanium discs were cleaned with acetone, 100% ethanol and deionized water in an ultrasonic bath for 10 mins. The procedure of sonication was repeated 3 times with fresh solution, for a total sonication time of 90 min and the disc were dried on a hot plate at 80

degree (**Fig. 4**). Then, titanium samples were placed on a petri dish and placed in an oxygen plasma cleaner (Harrick Plasma Cleaner, PDC-002,230 V). High-pressure oxygen plasma was applied for 10 minutes to functionalize the surfaces with hydroxyl groups (**Fig. 4A**). Afterwards, plasma treated substrates were removed and placed in a desiccator and 300  $\mu\text{l}$  of TPFS was placed next to the samples. The silanization reaction was carried out for 3 h at room temperature through CVD (**Fig. 4B**), followed by heat treatment at 60 °C overnight to finish the reaction. After the heat treatment silanized surfaces were placed in a desiccator and pumped under vacuum (with the exist valve open) for 10 min to remove unbonded silane molecules. (**Fig. 4C**). Before performing the experiments, 80  $\mu\text{l}$  PFPP lubricant was infused on each sample to create the LIS (**Fig. 4D**).

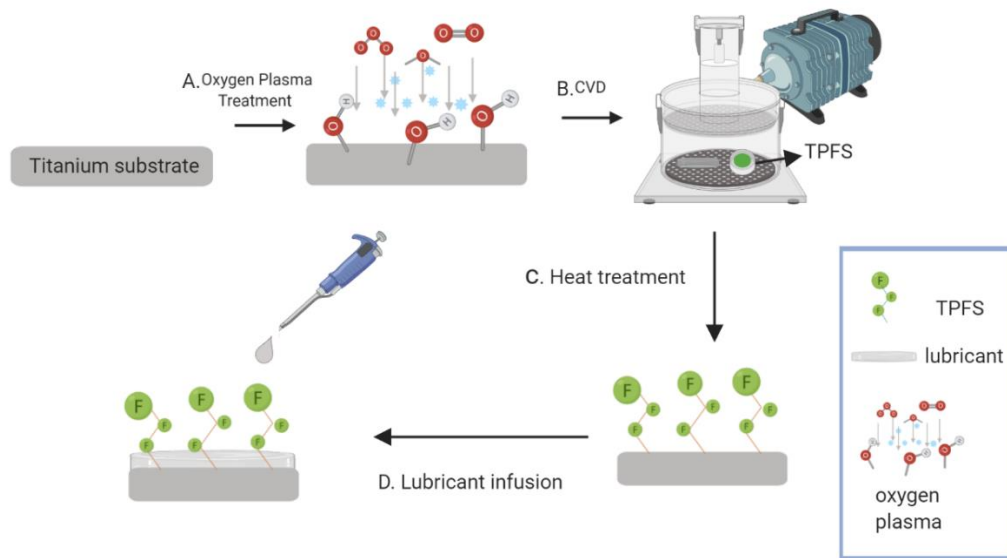


**Figure 4.** Schematic representation of preparing LIS on titanium substrates.

### 3.2.2 Biofunctionalized lubricant-infused chitosan-GPTMS crosslinked coating

Titanium surfaces went through washing, sonication and oxygen plasma treatment as explained in the section 3.2.1. The surface modification aims to immobilize chitosan on titanium surfaces, so GPTMS was used as a silane coupling agent and cross-linked with chitosan to prepare the chitosan-GPTMS mixture. After plasma treatment, titanium surface was cured with chitosan-GPTMS solution and heat treated at 60 °C overnight to finish the crosslinking reaction. The amine groups present on chitosan were bond to the epoxy groups on the silane and formed a layer on titanium surface. (**Fig. 5A and B**)

To prepare the mixture, 2.5% chitosan was dissolved in 1% acetic acid solution and mixed with GPTMS, reaching a 75 wt% chitosan in the chitosan and GPTMS mixture. Approximately 100  $\mu$ l of the chitosan-GPTMS mixture was added on each oxygen plasma activated titanium sample.

To obtain LIS on chitosan coated titanium surfaces, a secondary oxygen plasma treatment was performed on the chitosan-GPTMS coated surfaces to partially etch the surface and generate hydroxyl functional groups. Then, samples were CVD treated with TPFS, as illustrated in **Fig. 5C-D**. Surfaces were then heat treated as explained in section 3.2.1. Afterwards, lubricant was infused into the substrates prior to performing the following experiments described in chapter four (**Fig, 5E and F**).

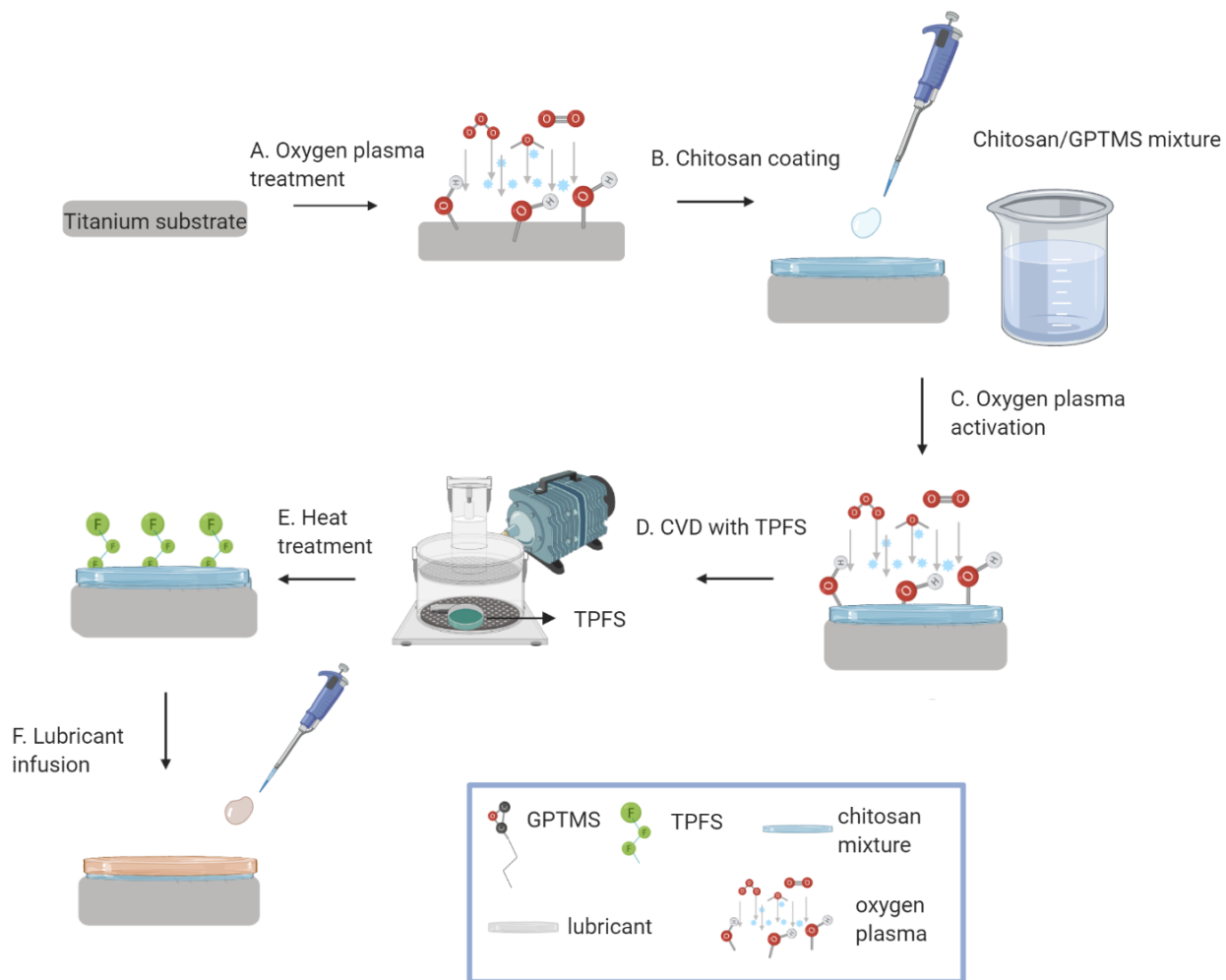


**Figure 5.** Schematic representation of creating biofunctionalized lubricant-infused chitosan-GPTMS crosslinked coating.

### **3.2.3 Layer-by-layer biofunctionalized lubricant-infused DHB-chitosan conjugated coating**

Titanium surfaces went through washing, sonication and oxygen plasma treatment as explained in section 3.2.1. Preparation of chitosan lay-by-layer dip coating on titanium is illustrated in **Fig. 6**. Chitosan was conjugated with dihydroxybenzaldehyde (DHB) and bound to titanium surface through a strong electrostatic coupling generated between the catechol groups on the DHB molecule and the negatively charged titanium alloy. Chitosan powder was dissolved in 1% acetic acid solution at 40 °C and stirred at 600 rpm for 3 h. Subsequently, chitosan and DHB conjugated solution was obtained by mixing chitosan and DHB at a mass ratio of 1:2 overnight at 37 °C and stirred overnight. Afterwards, impurities were separated from 8 g/l chitosan-catechol conjugated solution by 4 min centrifugation at 500 XR. (**Fig. 6A**). Then, samples were dip-coated in clear chitosan-catechol conjugated solution and dried at 60 °C on a hot plate for 3h. The dip coating procedure was repeated for 3 times followed by 5 min ultrasonication and dried at 60 °C on a hot plate (**Fig. 6B**). Then, samples were immersed in 0.01M NaOH solution with ethanol to neutralize the acetic acid, followed by washing with DI water and dried on a hot plate at 60 °C for 3 h.

To prepare LIS on chitosan coated titanium samples, samples were oxygen plasma treated for 10 min to functionalize surfaces with hydroxyl groups (**Fig, 6C**). Afterwards, plasma treated substrates were placed in a desiccator with 300  $\mu$ l of TPFS in petri dish placed next to samples. The salinization reaction was carried out for 3 h at room temperature through CVD method (**Fig. 6D**), followed by 60 °C heat treatment overnight to finish the reaction.

Then, unbonded silane were removed by 10 min vacuuming. Afterwards, 80  $\mu\text{l}$  PFPP lubricant was infused on each sample before each experiment. (**Fig. 6E**)

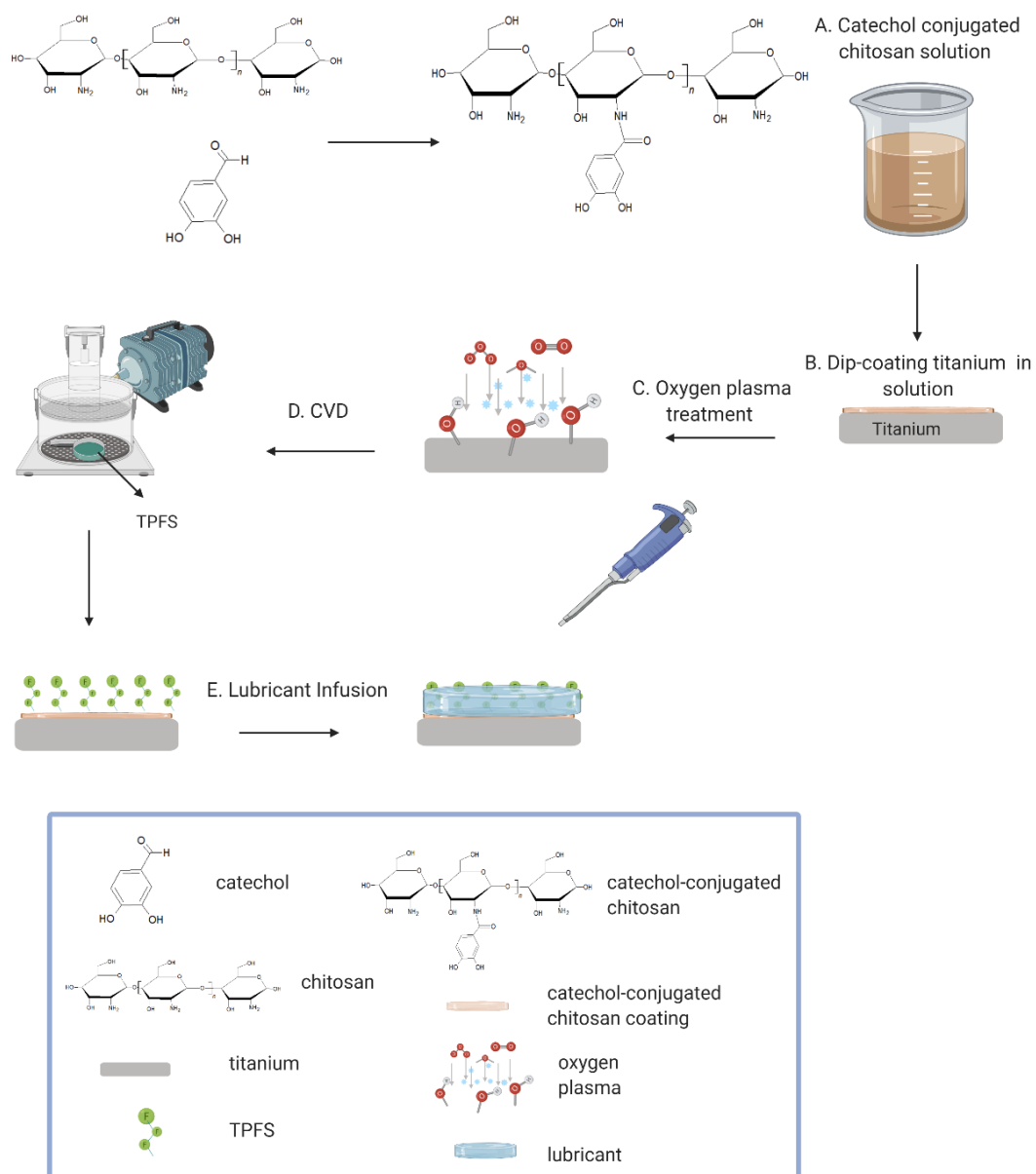


**Figure 6.** Schematic representation of creating a layer-by-layer biofunctionalized lubricant-infused DHB-chitosan conjugated coating.

### **3.2.4 Biofunctionalized lubricant-infused chitosan conjugated coating created using mixed silanes**

Titanium surfaces went through washing, sonication, and oxygen plasma treatment as explained in previous procedures described in section 3.2.1.

Given that GPTMS can provide anchors for bioconjugation with chitosan and TPFS can maintain repellency of surface, GPTMS and TPFS were used to treat titanium surface during CVD process simultaneously at ratio of 75:25 to create the bio-functional lubricant-infused titanium surfaces. Firstly, titanium samples were put in an oxygen plasma cleaner (Harrick Plasma Cleaner, PDC-002, 230 V) and high-pressure oxygen plasma was applied on samples for 10 min to functionalize surfaces with hydroxyl groups (**Fig. 7A**). After surface activation, samples were placed in a desiccator and CVD treated with a 75%-25% volume ration of GPTM and TPFS respectively. The silanes were placed on two small glass slides separately put next to the samples. The CVD treatment was carried out for 5 h and followed by heat treatment at 60 °C heat overnight to finish the reaction. Unbonded silane molecules were removed by 10 min post vacuuming in a desiccator (**Fig. 7B and C**).

Chitosan powder was dissolved in 1% acetic acid solution at 40 °C and stirred at 600 rpm for 30 min to form 50 µg/ml chitosan solution. Titanium surfaces functionalized with the mixed silanes monolayer were put in a 48 well plate and 500 µl chitosan solution was added to each well. The well plate was kept at 4 °C for 12 h to complete the bioconjugation. Later the samples were washed with PBS and kept at 4 °C before next the steps (**Fig. 7D**). 80 µl PFPP lubricant was added on each sample before performing the experiments (**Fig. 7E**).

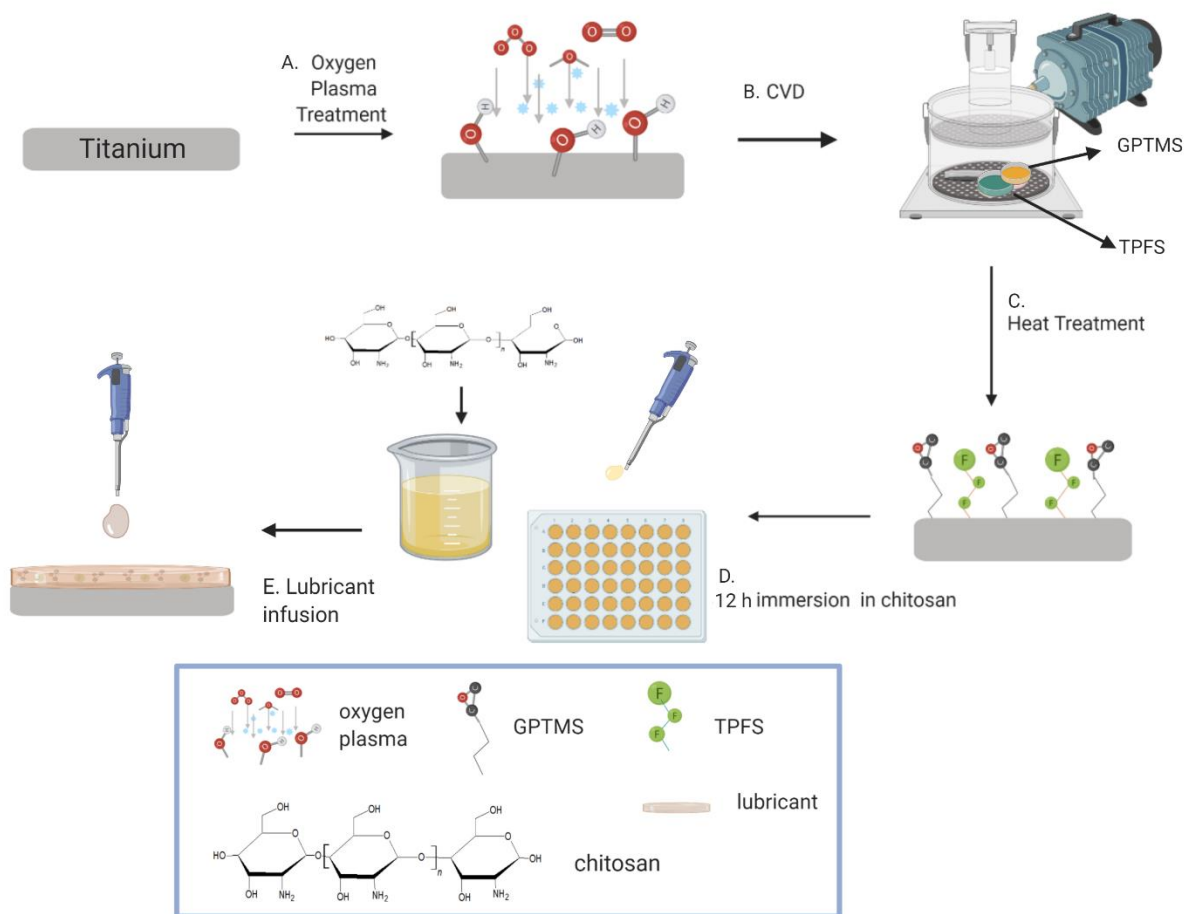


**Figure 7.** Schematic representation of creating bio-functional lubricant-infused chitosan conjugated surfaces using mixed silanes.

### **3.2.5 Biofunctionalized lubricant-infused collagen conjugated coating created using mixed silanes**

Titanium surfaces were washed, sonicated and oxygen plasma treated as previously explained in section 3.2.1. In this modification procedure, instead of GPTMS, APTES was used as the optimal coupling agent for conjugating collagen on surfaces coated with a mixed APTES-TPFS monolayer. TPFS locks-in the lubricant layer, providing the LIS with desired repellency properties. A 75%-25% volume ratio of APTES and TPFS was used in this reaction.

Titanium samples were washed, sonicated and oxygen plasma treated as explained in section 3.2.1. Clean samples were put in an oxygen plasma cleaner and high-pressure oxygen plasma was applied on samples for 10 min to functionalize surfaces with hydroxyl groups (**Fig. 8A**). After plasma treatment, samples were placed in the desiccator and CVD treatment was performed with 75%-25% APTES-TPFS. The operation was carried out for 5 h (**Fig. 8B**), followed by heat treatment at 60 °C overnight to finish the reaction. At the final step, samples were vacuumed in desiccator for 10 min to get rid of unbonded silane molecules (**Fig. 8C**).

To biofunctionalized surfaces with collagen, 50  $\mu\text{g/ml}$  collagen was mixed with 10 mM EDC and 25 mM NHS in DI water and added to mixed silane modified titanium substrates. The substrates were incubated in 48 well plate at 4 degree for 12 h with 500  $\mu\text{l}$  of collagen solution in each well. After the coating process, samples were washed with PBS and were dried at 37 °C for 30 min, stored at 4 °C. The preparation process is described in **Fig. 8D**.

80  $\mu\text{l}$  PFPP lubricant was added on each sample prior to performing the following experiments (**Fig. 8E**).

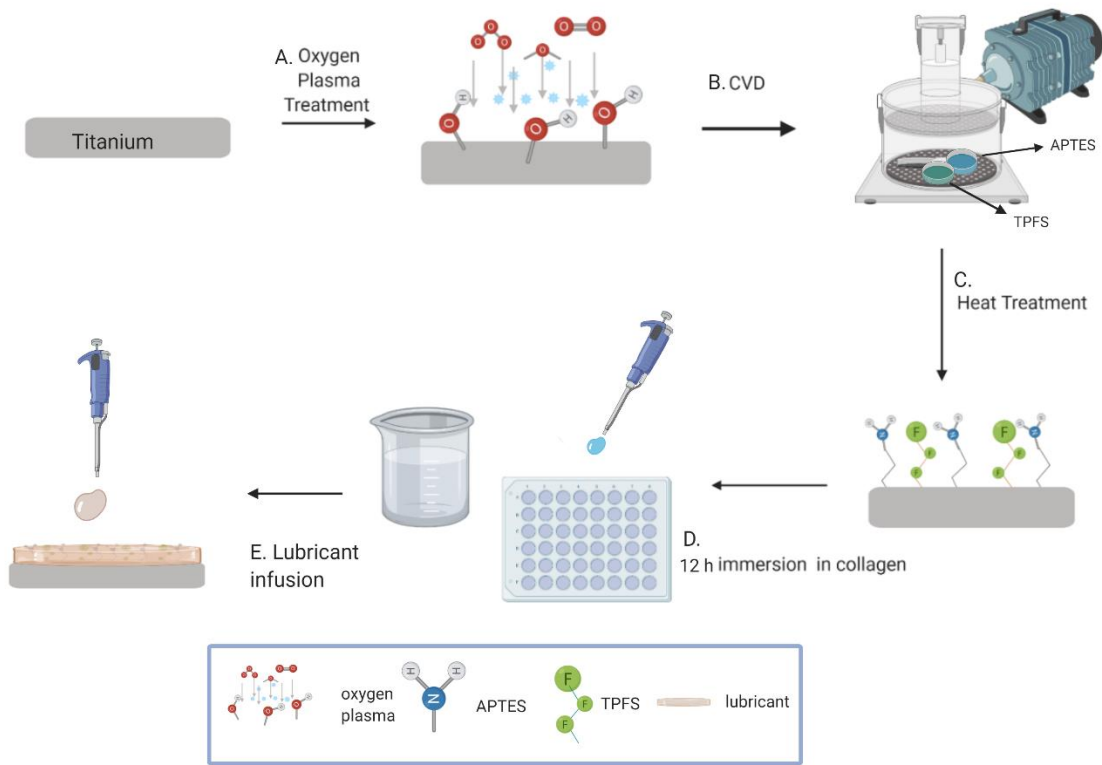


**Figure 8.** Schematic representation of creating biofunctionalized lubricant-infused collagen conjugated coatings using mixed silanes.

### **3.2.6 Contact and sliding angle measurement**

To investigate the hydrophobicity and slippery property of control and modified substrates, 5  $\mu\text{l}$  Milli-Q water droplets were used to perform static contact and sliding angle measurement. The Future Digital Scientific OCA20 goniometer (Garden City, NY) was used to measure water sessile drop contact angle at room temperature with calibration step prior to measurement.

The sliding angles were measured by digital angle level (ROK, Exeter, UK). PFPP lubricant was added to samples before measurement. Due to high viscosity and low vapor pressure, lubricant layer on samples could maintain stability. Each sample is added with PFPP and placed on a calibrated level, then a 5  $\mu\text{l}$  droplet of deionized water was placed on each sample. When gently angled the calibrated level, the minimal angle that made droplet started sliding on the surface of each sample was recorded as sliding angle. If droplet failed to slide at angle of 90 degree or higher than it, the sliding angle was recorded as 90 degree. The measurements were repeated for 3 times on each sample and three samples were used in each control group.

### 3.2.7 Biofilm formation

To test the biofilm formation on control groups, biofilms were grown on surfaces and adhered biomass was visualized by crystal violet staining. MW2 strain *staphylococcus aureus strain* (*S. aureus*) were used. In each type of surface, 2 samples were used as blank. *S. aureus* was made in Luria-Bertani medium (LB) through overnight cultivation. Bacteria were grown over night and then were diluted at 1:100 bacteria: fresh media. After being cultivated in fresh LB media and grew for 2.5 h until it reaches  $\sim OD_{600} = 0.4$ , measured by plate reader. Then bacteria were seeded with TSBC5 media (Tryptic Soy broth with 0.5% glucose, 0.2% sodium citrate, 0.6% yeast extract) at 1: 50 ratio and added to a 48 well plate with samples. 350  $\mu l$  mixed solution was put in each well and incubated at 37 °C in a shaking incubator at 30 rpm.

After 48 h bacteria culture with two bacteria strains, samples were gently washed in PBS solution and put into a clean 24 well plate, followed by adding 700 ml crystal violet (CV) to stain samples for 15 min. After removing CV, added DI water 700 ml and remove to wash samples. This procedure was repeated until there was no more CV dilute into DI water. Then, samples were air dried for one day under room temperature. 700  $\mu l$  of 30% acetic acid was added to each sample and completely dissolved CV into acid solution for 20 min. Pipette was used to mix solution in each well homogeneously and take 250  $\mu l$  solution from each sample to a 96 well plate. The absorbance of CV was measured at 590 nm using a microplate spectrophotometer (Bio-Rad Laboratories, CA, USA). Finally, optical density

obtained from CV light absorption on experimental group was subtracted by that on corresponding blank sample which were cultured without bacteria.

### **3.2.8 Cell adhesion and bio-functionality of modified titanium surfaces**

Saos-2 osteosarcoma cells (ATCC<sup>®</sup>) were cultured in mixed McCoy's modified 5A media which was supplemented with 15% fetal bovine serum (FBS) and 1% streptomycin. Saos-2 cells were cultivated in an incubator at 37 degree and 5% CO<sub>2</sub> with their media being changed every 3 days. When cells became confluent, cells were detached by Trypsin-EDTA and prepared for experiments.

The experimental groups involved samples prepared by GPTMS crosslinking method described in section 3.2.2, dip-coating method in section 3.2.3 and mixed silane modifications described in section 3.2.4 and 3.2.5. Modified surfaces without lubricant infusion, LIS modified titanium and untreated titanium samples were used as control groups.

To test osteoblast inductive property of titanium that went through different treatments, samples were transferred into 24 well plates followed by adding a specific number of Saos-2 cells. In the first round of cell culture experiment (lubricant-infused chitosan-DHB coated titanium surfaces), 100  $\mu$ l of  $2 \times 10^5$  cells/ml SAOS-2 in media was added into each well, counted by hemocytometer. Samples were cultured with cell medium at 37 °C in an incubator and the cell medium was changed every 5 days. In next round experiment (lubricant-infused surfaces created by mixed silanes),  $8 \times 10^4$  cells/ml SAOS-2 cells in media was added into each well cultured with samples.

After culturing for a specific culture time, samples were washed with PBS twice to remove unattached cells. After washing cells with PBS, adherent cells were fixed, permeabilized, blocked with 4% formalin, 0.1% Triton x-100 and 4% BSA solution, respectively. Finally, DAPI and phalloidin solution were used to stain cell nucleus and actin filament and the surfaces were imaged with a fluorescence microscope where the potency of each surface for cell adhesion and repellency was evaluated. The number of adherent cells on different surfaces were measured using ImageJ software.

## CHAPTER FOUR: RESULTS AND DISCUSSION

### 4.1 Surface Wettability

#### 4.1.1 Wettability of lubricant-infused titanium surfaces

As seen in **Fig. 9A**, treated and untreated substrates exhibit different wettability properties. In **Fig. 9**, diagram shows static contact angles of  $5\ \mu\text{l}$  Milli-Q water droplets on untreated titanium control group (Ti) and TPFS modified titanium experimental group (Ti-FS). Ti-FS treated surfaces were hydrophobic and their static contact angles was  $107.28 \pm 1.57^\circ$ , prior to adding the lubricant. Additionally, Ti-FS group showed significant increase of contact angle from that on Ti control group which was  $40.58 \pm 2.52^\circ$  with ( $P < 0.01$ ). The increased hydrophobicity of Ti-FS treated surfaces reveals a successful CVD process that functionalized titanium surface with TPFS which changed the surface wettability titanium from hydrophilic to hydrophobic.

Moreover, sliding angle on Ti-FS and Ti control group after adding lubricant layer are shown in **Fig. 9B**. On Ti control group, droplets did not slide and sliding angles were recorded as  $> 90^\circ$ . In contrast, lubricated Ti-FS samples (Ti-FS+L) exhibited slippery properties and significantly decreased the sliding angles compared with lubricated control Ti (Ti+L) surfaces ( $7.06 \pm 1.28^\circ$ ). These results confirmed that, similar to previously reported LIS,<sup>132–134</sup> Ti surfaces were successfully functionalized with a lubricant-infused layer and showed water repellency and slippery properties.

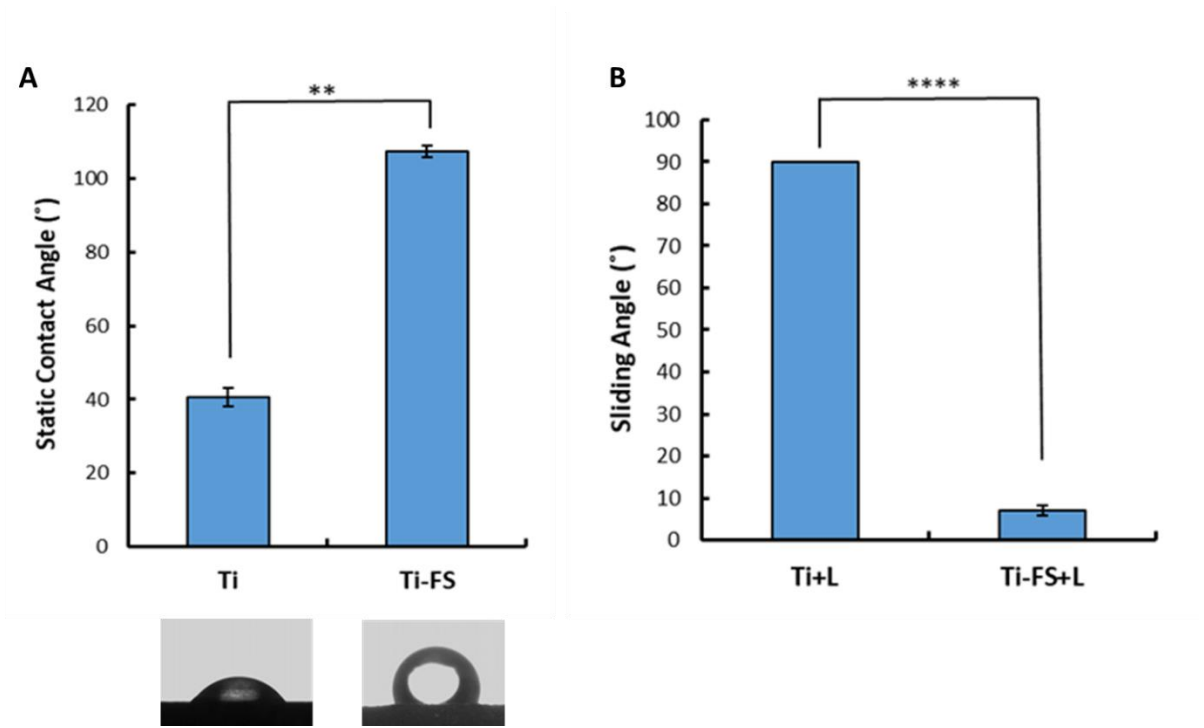


**Figure 9.** The contact angle and sliding angle measurements of water droplet on untreated titanium (Ti), and TPFS modified titanium samples (Ti-FS), **A**) static contact angle results of surfaces before adding lubricant layer, **B**) sliding angle results of the surfaces after adding the lubricant layer. Each group has three samples and each sample was measured for three times. Error bars represent the standard deviation (SD) of the mean of at least three samples. \*\* $P < 0.01$  and \*\*\*\* $P < 0.0001$  compared with Ti control samples.

#### 4.1.2 Wettability of chitosan coated titanium surfaces

As shown in **Fig. 10A and B**, GPTMS crosslinked chitosan on titanium (chitosan-GPTMS) and DHB bonded chitosan on titanium (chitosan-DHB) were used as control groups. TPFS modified GPTMS and DHB were used as experimental groups (chitosan-GPTMS-FS and chitosan-DHB-FS respectively).

The static contact angle on chitosan-GPTMS control group was  $46 \pm 3.33^\circ$  and significantly increased to  $100.76 \pm 3.4^\circ$  on chitosan-GPTMS-FS treated samples ( $P < 0.001$ ). Similarly, the static contact angle on chitosan-DHB-FS group was significantly higher when compared with chitosan-DHB modified surfaces ( $107.62 \pm 1.33^\circ$  and  $80.08 \pm 2.25^\circ$  respectively,  $P < 0.01$ ).

The results obtained from the contact angle measurements confirmed that TPFS monolayer had been successfully immobilized on chitosan coated surfaces of both chitosan-GPTMS and chitosan-DHB samples after CVD treatment with TPFS. Additionally, the hydrophobicity of chitosan coated titanium was increased to the level of TPFS modified titanium surfaces (data shown in section 4.1.1) which indicates that the presence of the chitosan coating did not influence the effect of TPFS modification on the substrates.

To illustrate the slippery properties of control samples, PFPP lubricant was added to samples and sliding angle measurements were performed using a  $5 \mu\text{l}$  water droplet. The minimum angle for droplets to begin sliding on substrate was defined as the sliding angle. When droplets failed to slide on the surfaces, at  $\geq 90^\circ$  tilting angle, a sliding angle of  $90^\circ$  was reported.

Sliding angles of water droplet on different surfaces are shown in **Fig. 10B**. The  $5\ \mu\text{l}$  water droplet did not slide on lubricated chitosan-GPTMS and chitosan-DHB treated control groups (tilting angles higher than  $90^\circ$ ), suggesting that these surfaces do not have slippery properties. In contrast, lubricated chitosan-GPTMS-FS and chitosan-DHB-FS surfaces (chitosan-GPTMS-FS+L and chitosan-DHB-FS+L) significantly decreased the sliding angles and showed water repellency properties (sliding angles at  $16.33 \pm 4.38^\circ$  and  $11.18 \pm 2.52^\circ$  respectively), compared with the control groups.

Water repellency and slippery properties are major characteristics of LIS.<sup>132-134</sup> Low sliding angles seen on lubricant-infused, TPFS modified surfaces indicate that the TPFS monolayer was successfully immobilized on titanium samples coated with chitosan *via* two different modification procedures (described in sections 3.2.2 and 3.2.3).

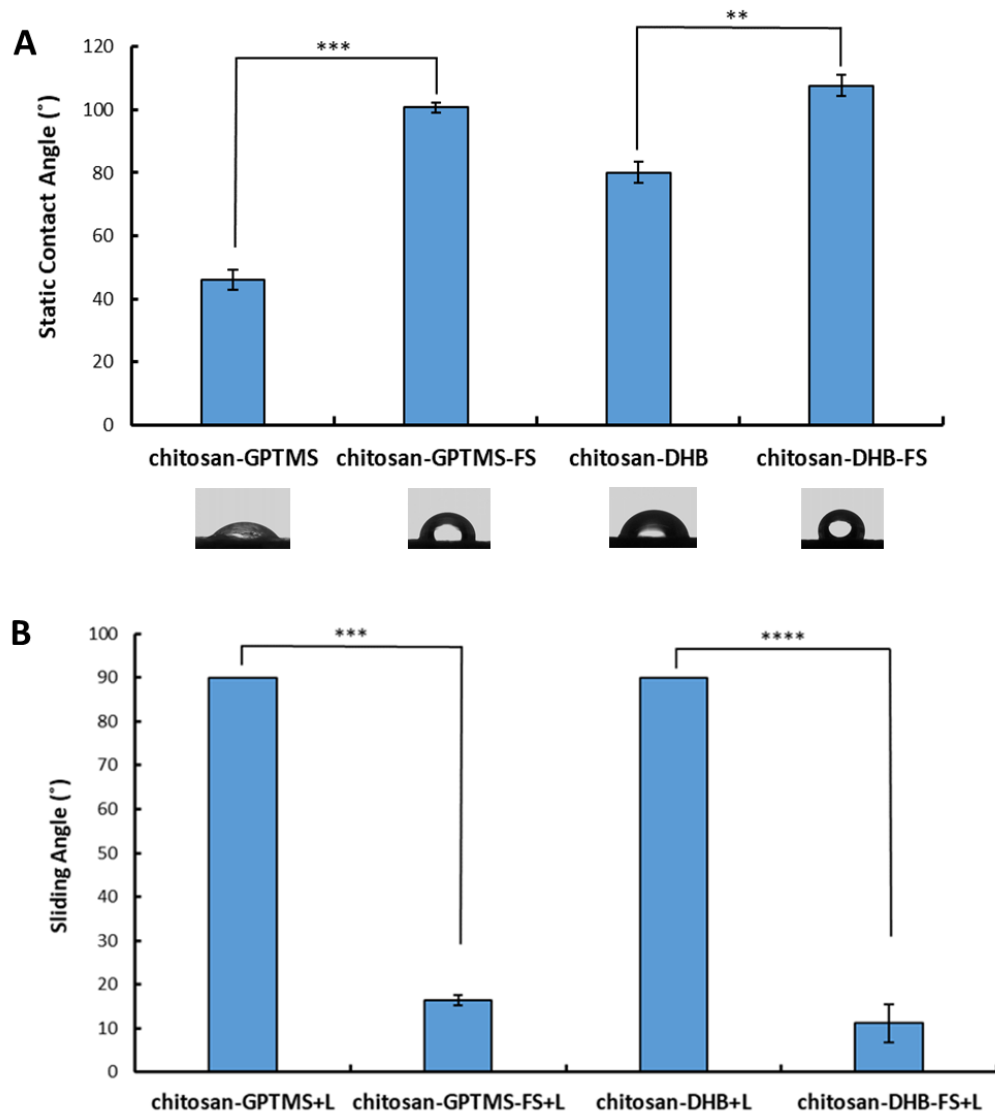


**Figure 10** The contact angle and sliding measurements of water droplet on control and experimental groups, **A)** Static contact angle results of surfaces before adding lubricant layer, **B)** Sliding angle results of the surfaces after adding the lubricant layer. Each group has three samples and each sample was measured for three times. Error bars represent the SD of the mean of at least three samples. \*\*\*  $P < 0.001$  and \*\*\*\*  $P < 0.0001$  when compared with chitosan-GPTMS and chitosan-DHB respectively.

#### 4.1.3 Wettability of mixed silanes modified titanium surface

Water contact angles on control and experimental groups are revealed in **Fig. 11A**. In this section, titanium samples modified with 100% GPTMS (GPTMS100) and 100% APTES through CVD (APTES100) were used as control groups. Experimental groups included titanium samples modified with 75%GPTMS-25%TPFS (GPTMS75-TPFS25) and titanium modified with 75%APTES-25%TPFS (APTES75-TPFS25).

The static contact angle measurements of the control and experimental groups before adding the lubricant layer are shown in **Fig. 11A**. Experimental groups exhibited high contact angles, confirming the hydrophobic properties of mixed silanes treated samples. The static water contact angle on GPTMS75-TPFS25 significantly increased to  $117.45 \pm 0.67^\circ$  from  $47.35 \pm 2.12^\circ$  on GPTMS100 control group ( $P < 0.0001$ ). On APTES75-TPFS25 experimental group, contact angles were significantly higher ( $P < 0.0001$ ) than that on APTES100 control group ( $118.98 \pm 0.21^\circ$  and  $19.4 \pm 1.25^\circ$  respectively). In contrast to the excellent water repellency properties seen in APTES75-TPFS25 treated samples, APTES100 surfaces were hydrophilic and the water droplets immediately spread on these surfaces, covering, and wetting the entire substrate.

The contact angle measurements obtained from APTES100 and GPTMS100 control groups illustrates that adding a certain ratio of APTES or GPMMS to the TPFS monolayer structure does not affect the hydrophobicity of the TPFS layer and 25% TPFS is sufficient to make the surfaces repellent and hydrophobic. In addition, no significant difference was seen in

the hydrophobicity properties of mixed silane treated surfaces when compared to substrates treated with 100% TPFS (section 4.1.1).

After the addition of PFPP lubricant layer to control and experimental groups, sliding angles were measured (**Fig. 11B**). The 5  $\mu$ l water droplet did not slide on lubricated control groups, suggesting that these surfaces do not have slippery properties. In contrast, as shown in **Fig. 11B**, sliding angles significantly decreased in lubricant-infused GPTMS75-TPFS25+L and on APTES75-TPFS25+L samples ( $26.51 \pm 1.64^\circ$  and  $14.40 \pm 1.12^\circ$  respectively,  $P < 0.0001$ ).

In conclusion, after adding the lubricant layer, experimental groups exhibited excellent lubricant-infused characteristics and their repellency properties were like those of Ti-FS+L treated surfaces described in section 4.1.1.

This was also seen in a previous study conducted in our group where bio-functional lubricant-infused surfaces were created using APTES and TPFS mixed silanes.<sup>133</sup> In this study, it was shown that the repellency and blocking properties of lubricant-infused layer was not compromised when mixing the TPFS layer with APTES. LIS with APTES enabled anchoring biomarkers and biofunctionalized LIS were successfully created.

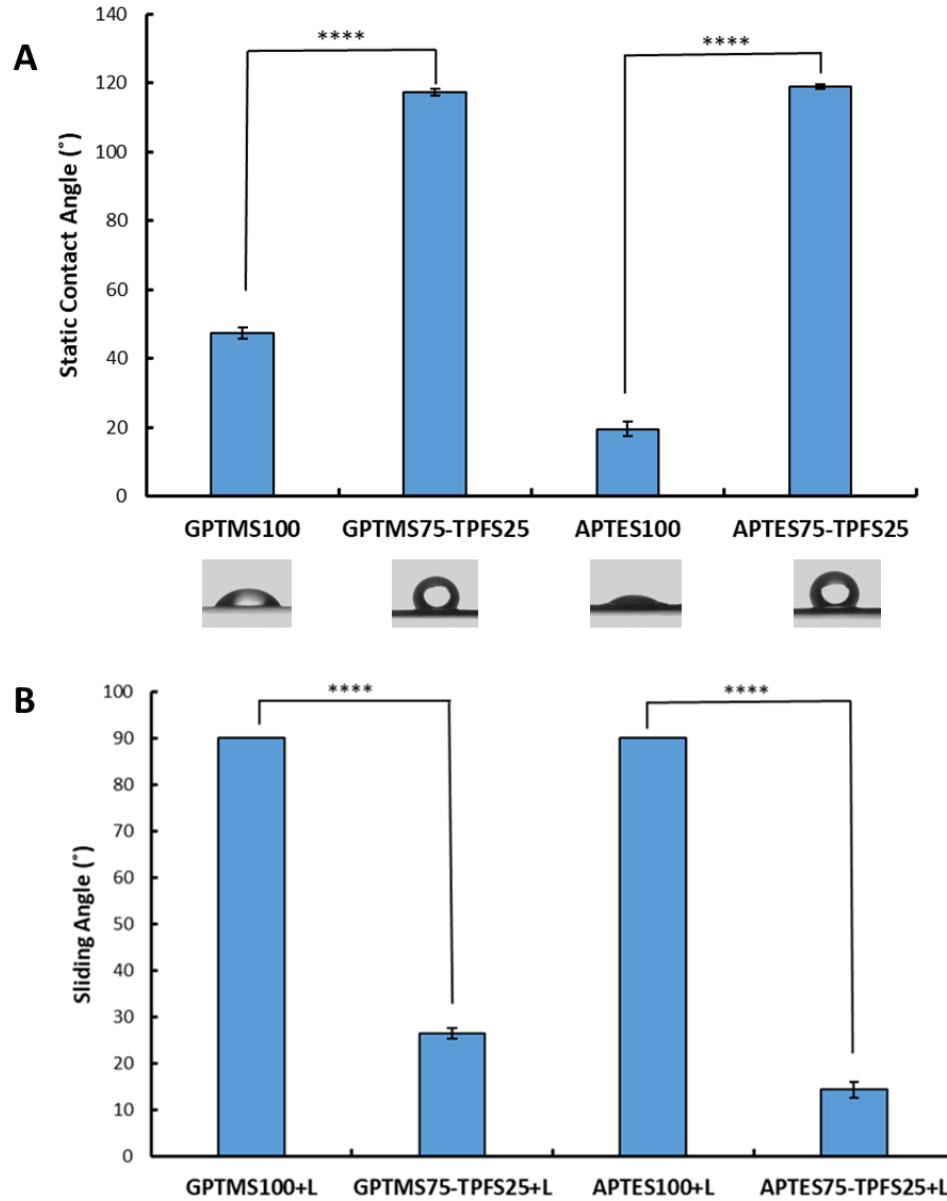


**Figure 11.** The contact angle and sliding measurements of water droplet on control and experimental groups, **A)** static contact angle results of surfaces before adding lubricant layer, **B)** sliding angle results of the surfaces after adding the lubricant layer. Each group has three samples and each sample was measured for three times. Error bars represent the SD of the mean of at least three samples. \*\*\*\*  $P < 0.0001$  when compared with control samples.

## 4.2 Anti-biofouling Properties

### 4.2.1 Bacteria repellency properties of LIS modified titanium substrate

*S. aureus* was used to form biofilms on untreated titanium (Ti) TPFS modified (Ti-FS) and lubricant-infused titanium surfaces (Ti-FS+L).

The CV absorbance of stained biofilm on Ti-FS+L samples was significantly lower than that on Ti and Ti-FS experimental groups ( $P < 0.01$ ). However, concentration of attached *S. aureus* was found to be relatively high on hydrophobic TPFS modified samples with no lubricant (Ti-FS). According to the discovery from Kochkodan *et al.* lab<sup>135</sup> and Giaouris *et al.* lab<sup>136</sup>, hydrophobic cells have stronger adherence to hydrophobic surfaces and hydrophilic cells strongly attach to hydrophilic surfaces. The surface energy of bacteria is typically lower than that of human body fluid and they show high affinity towards hydrophobic materials.<sup>137</sup> No statistical difference was observed between the biofilm biomass of the Ti control and Ti-FS experimental groups.

The concentration of adherent bacteria was significantly lower on Ti-FS+L samples compared with Ti-FS and untreated titanium substrates ( $P < 0.01$ ). This indicates the excellent antifouling and blocking properties of lubricant-infused Ti surfaces. Furthermore, resistance and removal of bacteria on LIS surface is contributed to the high mobility and dynamic feature of the lubricant layer present on slippery lubricant interface.<sup>45</sup>

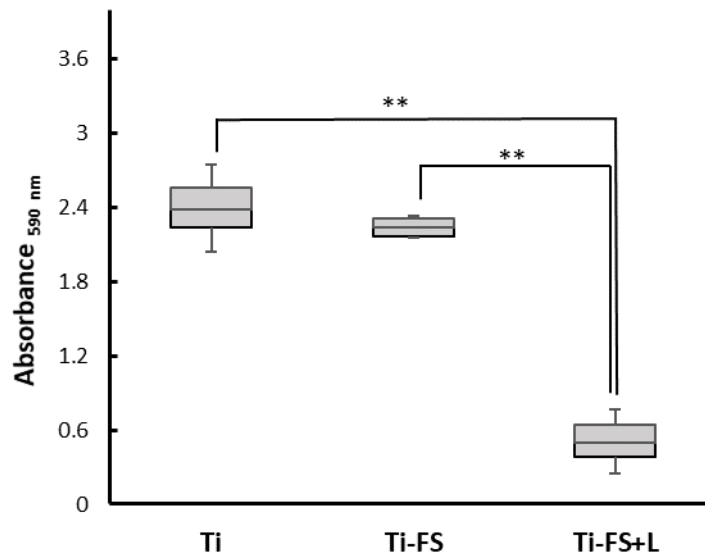


**Figure 12.** Results obtained from the bacterial adhesion studies on uncoated and coated Ti substrates using crystal violet staining assay. Ti-FS+L surfaces significantly prevented bacterial adhesion and biofilm formation when compared to untreated Ti and Ti-FS surfaces. Whiskers span the first quartile and fourth quartile range of at least 3 samples. \*\*  $P < 0.01$  when compared with Ti-FS+L samples.

#### **4.2.2 Bacteria repellency of chitosan modified titanium surfaces using GPTMS and DHB crosslinking**

In these experiments, Ti, and Ti-FS+L, titanium substrates coated with chitosan by GPTMS crosslinking method (chitosan-GPTMS) and titanium coated with chitosan-DHB conjugation *via* the layer-by-layer dip-coating method (chitosan-DHB) were used as control groups. The experimental groups were LIS modified GPTMS samples (chitosan-GPTMS-FS+L) and LIS modified DHB samples (chitosan-DHB-FS+L). Results were obtained from measuring CV light absorbance at 590 nm.

As seen in **Figure 14**, bacteria viability was not inhibited on chitosan-GPTMS-FS+L samples, but CV absorbance was significantly reduced in chitosan-DHB-FS+L samples compared with Ti and chitosan-DHB control groups ( $P < 0.05$ ). Moreover, the coating on chitosan-GPTMS and chitosan-GPTMS-FS+L was not stable and broken and detached chitosan membranes were observed on these samples after performing the bacterial adhesion studies (**Fig. 13A**). In contrast, the coating on chitosan-DHB and chitosan-DHB-FS+L samples was more stable during the experimental process (**Fig. 13B**).

LIS modification on GPTMS samples did not improve the anti-biofouling properties of the coated surfaces. This may be attributed to the fast biodegradation and detachment of the crosslinked layer in the bacteria environment and as a result the detachment of the lubricant-infused layer from the surface. According to the results obtained from these experiments it could be concluded that the method of crosslinking chitosan to form a thick layer on

titanium and modifying the crosslinked membrane with a lubricant-infused layer is not a suitable and feasible method for creating bio-functional LIS on titanium samples.

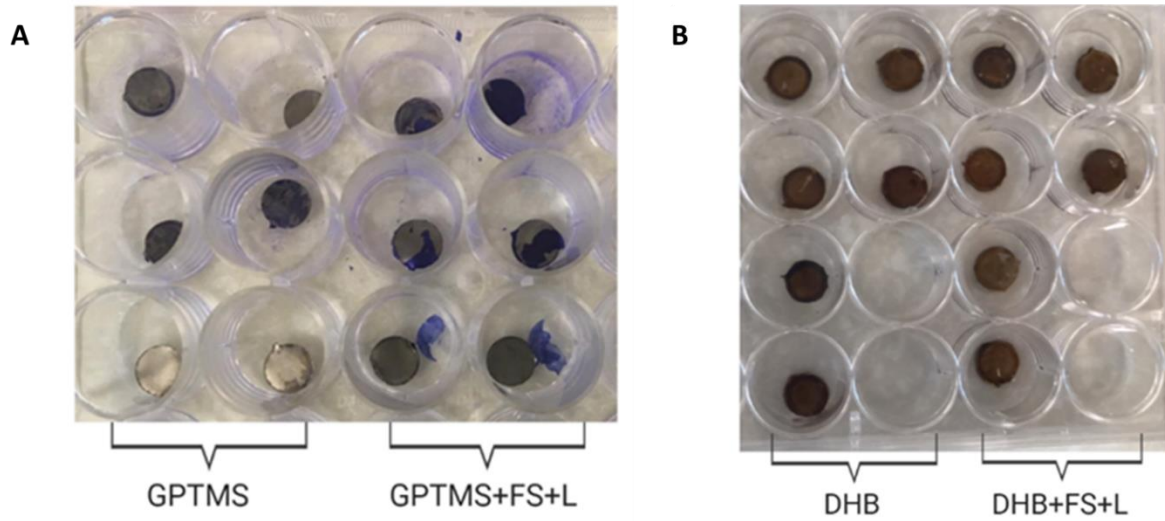


**Figure 13.** Crystal violet staining assay for investigating the antifouling properties of the modified surfaces, **A)** detachment of membrane observed on chitosan-GPTMS and chitosan-GPTMS-FS+L groups, **B)** Stability of chitosan-DHB and chitosan-DHB-FS+L samples after biofilm experiment.

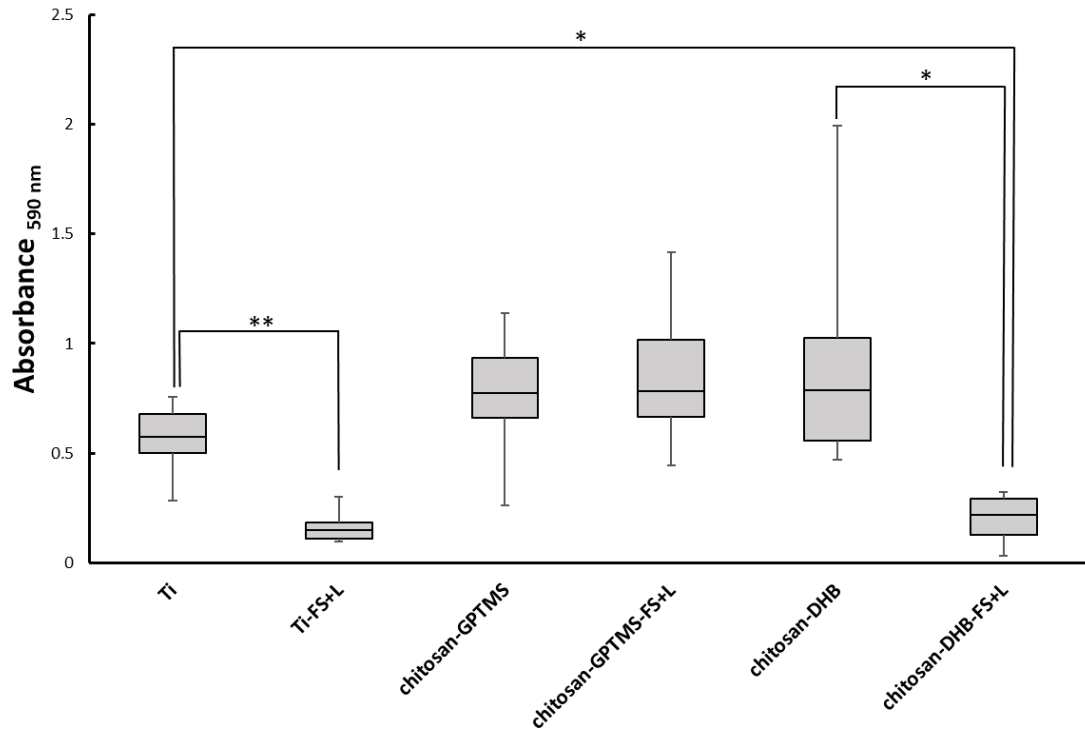


**Figure 14.** Crystal violet evaluation of *S. aureus* biofilm formation on control and experimental groups. Whiskers span the first quartile and fourth quartile range of at least 3 samples. \*\*  $P < 0.01$  and \*  $P < 0.05$  when compared with Ti and chitosan-DHB groups, respectively.

### **4.2.3 Bacteria repellency properties of mixed silane coated titanium surfaces biofunctionalized with chitosan or collagen**

Like the previous sections, Ti and Ti-FS+L were used as control groups in these experiments. Samples modified with mixed silanes of 75%-25% GPTMS-TPFS and 75%-25% APTES-TPFS were biofunctionalized with chitosan and collagen respectively and added with lubricant before bacteria cultivation (GPTMS75-TPFS25-chitosan+L and APTES75-TPFS25-collagen+L). Based on previous studies, GPTMS has been reported to be a suitable coupling agent for chitosan immobilization<sup>118,119,138</sup> and APTES for collagen immobilization.<sup>131,139,140</sup> GPTMS 100% and APTES 100% were also coated with chitosan and collagen respectively and used as control groups, labeled as GPTMS100-chitosan and APTES100-collagen respectively.

As seen in **Fig. 15**, the optical densities of solubilized CV on collagen control and chitosan control groups, were  $1.20 \pm 0.09$  a.u. and  $0.93 \pm 0.14$  a.u. respectively. High concentration of bacteria was seen on APTES75-TPFS25-collagen samples and these surfaces did not show bacterial repellency properties and no significant difference was seen when comparing the results with APTES100-collagen treated samples. These findings are inline with previous studies where collagen has shown to be bacterial friendly and the addition of collagen has shown to improve bacterial adhesion.<sup>141</sup> In contrast, GPTMS75-TPFS25-chitosan treated samples prevented biofilm formation and exhibited excellent bacterial repellency properties when compared with GPTMS100-chitosan treated samples ( $P < 0.01$ ) and control Ti substrates ( $P < 0.05$ ). In fact, GPTMS75-TPFS25-chitosan treated samples

suppressed bacterial adhesion and biofilm formation to Ti-FS+L levels and no significant difference was seen between these two groups. These results demonstrate that the antibacterial and blocking properties of the lubricant-infused layer has not been negatively impacted by the addition of chitosan.

Furthermore, when comparing the results obtained from collagen and chitosan coated surfaces, GPTMS75-TPFS25-chitosan+L treated surfaces significantly decreased bacterial adhesion compared with APTES75-TPFS25-collagen+L treated surfaces ( $P < 0.0001$ ), indicating that chitosan is a better biomarker than collagen for creating antifouling, bio-functional lubricant-infused surfaces.

In summary, the preliminary experiments performed on bio-functional lubricant-infused titanium surfaces obtained from different modification procedures indicate that Ti surfaces were successfully functionalized with TPFS demonstrated by the dramatic increase in contact angles (**Fig. 9A**). After adding the lubricant, TPFS functionalized titanium surfaces were able to lock-in the lubricant layer and they exhibited slippery properties as shown in **Fig 9B**. Further, Ti-FS+L showed significant resistance towards bacterial adhesion and biofilm formation when compared with Ti and Ti-FS groups (**Fig. 12**).

Additionally, the high contact angle measurements obtained from TPFS modified, GPTMS crosslinked chitosan coated titanium and DHB conjugated chitosan coated titanium samples (chitosan-GPTMS-FS and chitosan-DHB-FS respectively) high contact angles measurements obtained from these surfaces (**Fig, 10A**) confirm the successful immobilization of TPFS on chitosan modified titanium substrates. Then, their slippery

properties after adding the lubricant layer further confirmed the lubricant-infused properties of these surfaces (**Fig 10B**). These surfaces showed similar slippery properties to that of Ti-FS+L samples. However, when investigating the antibiofouling properties of the chitosan modified LIS, only chitosan-DHB-FS+L samples showed bacterial repellency properties and they attenuated bacterial adhesion to Ti-FS+L levels. (**Fig. 14**). In addition, these surfaces had a more stable surface coating when compared with GPTMS crosslinked chitosan coated substrates. (**Fig.13A and B**).

Furthermore, when looking at the results obtained from bio-functional lubricant-infused surfaces obtained using mixed silanes, both GPTMS75-TPFS25+L and APTES75-TPFS25+L surfaces exhibited slippery lubricant-infused properties (**Fig. 11B**). However, after bio-functionalizing these surfaces and when investigating the antifouling properties, only GPTMS75-TPFS25-chitosan+L showed antibacterial properties when compared to control groups (**Fig. 15**).

In conclusion, chitosan-DHB-FS+L and GPTMS75-TPFS25-chitosan+L modified surfaces exhibited superior antibiofouling properties when compared with other treated surfaces. Thus, these two modification procedures were selected and further tested for targeted cell adhesion and bio-functionality.

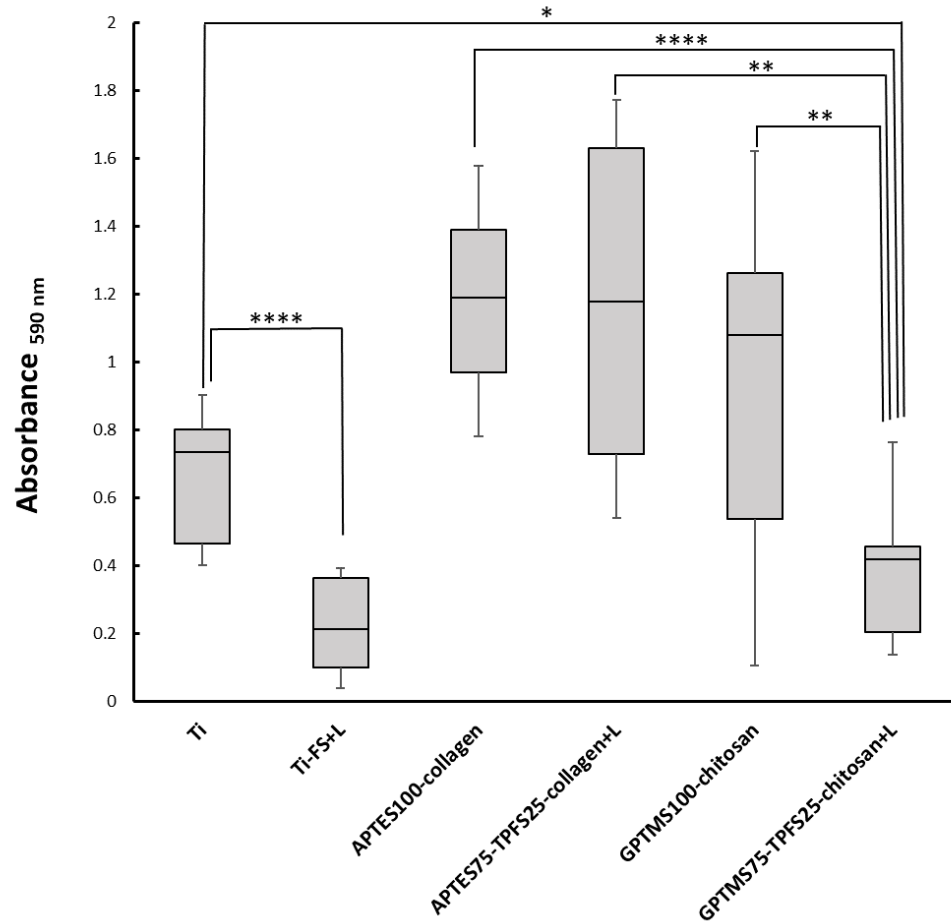


**Figure 15.** Crystal violet evaluation of *S. aureus* biofilm formation on control groups and experimental groups. Whiskers span the first quartile and fourth quartile range of at least 3 samples. \*\*\*\*  $P < 0.0001$ , \*\*  $P < 0.01$  and \*  $P < 0.05$  when compared with Ti and GPTMS75-TPFS25-chitosan+L group, respectively.

## 4.3 Cell adhesion experiments

### 4.3.1 Biofunctionalized lubricant-infused chitosan-DHB coated titanium surfaces

In cell culture experiments, samples were transferred into a 48 well plate and cultured with Saos-2 cells for 3 days. 0.1  $\mu\text{l/ml}$  DAPI was used to stain the nucleus and the cytoskeleton was stained with phalloidin. As seen in the representative fluorescence images in **Figure 16A** and the cell count results in **Figure 16B**, low cell adhesion and proliferation was seen on Ti-FS+L and chitosan-DHB-FS+L groups compared with chitosan-DHB and control Ti surfaces. Although, DHB-FS+L samples blocked cell adhesion to some extent, these surfaces promoted targeted binding and had significantly more adherent cells compared with Ti-FS+L samples ( $251 \pm 45$  cells/ $\text{mm}^2$  and  $32 \pm 6$  cells/ $\text{mm}^2$  respectively,  $P < 0.05$ ). Furthermore, Ti-FS+L samples exhibited superior blocking features when compared with unmodified control Ti surfaces ( $P < 0.01$ ). However, no significant difference was found between chitosan-DHB and chitosan-DHB-FS+L groups.

The ability for cells to spread on different samples was studied by performing immunofluorescence staining assays and fluorescence microscopy. (**Fig.17**). SAOS-2 cells were well adherent and spread on Ti samples and the filament network was formed around the cell nucleus. In contrast cell morphology remained circular on Ti-FS+L, chitosan-DHB and chitosan-DHB-FS+L groups and no obvious actin filament network was found on these surfaces. The actin filament formed by extended actin cytoskeleton around nucleus occurs during cell growth and maturation.<sup>142</sup> Additionally, differentiation of cells is also accompanied with the expansion of cell nucleus volume which is revealed in a previous

study reported by Omar F. Zouani *et al.*<sup>143</sup> As shown in **Fig. 17**, enlarged nucleus was found on control Ti surfaces but no obvious increased volume of cell nucleus was observed on chitosan-DHB, chitosan-DHB-FS+L and Ti-FS+L samples.

Catechol is reported to have a negative effect on cell growth by destroying the function of the cell membrane and inhibiting lipid peroxidation *via* redox cycling activity.<sup>144</sup> Although catechol has been widely applied in mucoadhesive chitosan for drug delivery<sup>145</sup> and tissue adhesives,<sup>146</sup> toxicity of catechol is indicated in rabbit, cat, rat, mouse and for human cell lines in several studies.<sup>147</sup> Bio-functional lubricant-infused chitosan-DHB conjugated titanium (DHB is a type of catechol) exhibited anti-biofouling properties by preventing biofilm formation and bacterial adhesion, and DHB conjugation increased cell numbers compared with LIS modified titanium surface. But it still lacks bio-functionality and osseointegration according to **Fig. 16B** where cell concentration on chitosan-DHB-FS+L was less than that on titanium control group. Additionally, the ability to form a confluent functional cell layer is a key requirement for titanium bone implant.<sup>76,77</sup> Given that growth and differentiation of cells are accompanied with cytoskeleton, nuclei and actin of cells elongation, filament network wrapped around the cell nucleus can reveal viability and differentiation of cells.<sup>142</sup> As it revealed in fluorescence images obtained after actin filament staining (red) in **Fig. 17**. Cell on chitosan-DHB-FS+L surface did not show well filament network around nucleus compared that on Ti surface.

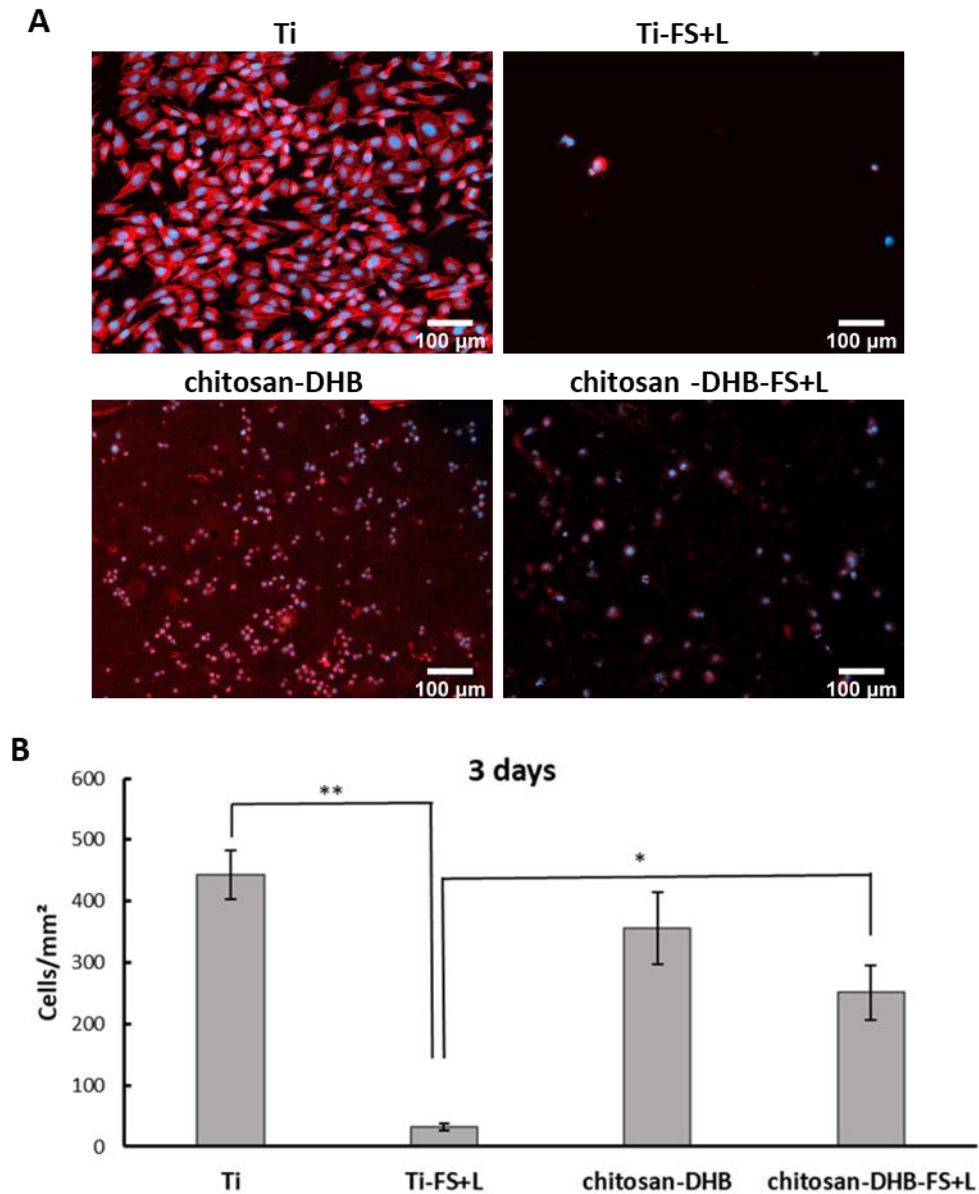


**Figure 16.** SaOS-2 cell proliferation after 3 days visualized by fluorescence spectroscopy (nuclei: blue; microfilaments: red) on the surface of control and experimental groups, **A**) Representative fluorescence images showing the density and distribution of adherent cells, **B**) statistical analysis of cell attachment and proliferation on different samples. Error bars represent the SD of the mean of at least three samples. \*\*  $P < 0.01$  and \*  $P < 0.05$  when compared with Ti-FS+L samples.

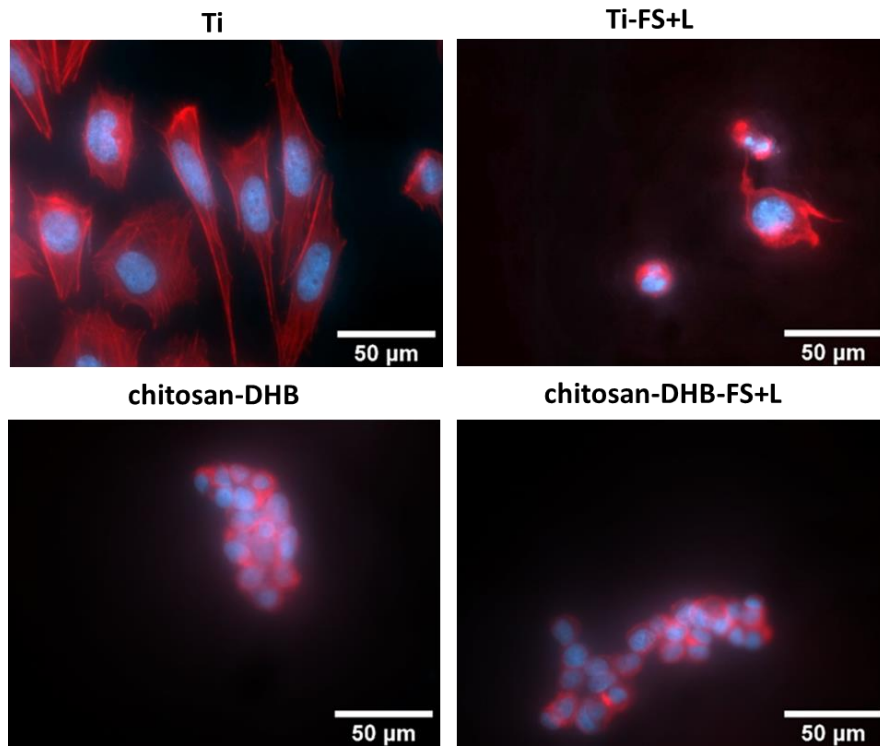


**Figure 17.** Immunofluorescence staining of cell nucleus and actin-based cytoskeleton (nuclei: blue; microfilaments: red) in human SAOS-2 cells to observe cell morphology and spreading.

#### 4.3.2 Bio-functional lubricant-infused surfaces created using mixed silanes

In this section, like the previous experiments, Ti and Ti-FS+L samples were tested as control groups and APTES100-collagen, APTES75-TPFS25-collagen+L, GPTMS100-chitosan, and GPTMS75-TPFS25-chitosan+L were tested as experimental groups. The mixed silanes method used to create bio-functional lubricant-infused surfaces is different from the method used in section 3.2.2 and 3.2.3 where titanium samples were initially coated with chitosan and then CVD treated with TPFS. Here, mixed silane surfaces were created by simultaneously modifying the substrates with a mixture of TPFS and the coupling agent (GPTMS or APTES) and subsequently immersing the samples in collagen or chitosan solutions. To complete the modification procedure, lubricant was then added to the substrates.

As seen in **Figure 18B** and **Figure 19B**, APTES100-collagen treated surfaces had the highest number of adherent cells ( $266 \pm 29$  cells/mm<sup>2</sup> and  $1325 \pm 135$  cells/mm<sup>2</sup>), followed by GPTMS100-chitosan treated surfaces ( $185 \pm 27$  cells/mm<sup>2</sup> and  $1030 \pm 133$  cells/mm<sup>2</sup>) after 3 and 7 days respectively. APTES75-TPFS25-collagen+L ( $160 \pm 10$  cells/mm<sup>2</sup> and  $1110 \pm 127$  cells/mm<sup>2</sup> after 3 days and 7 days respectively) and GPTMS75-TPFS25-chitosan+L surfaces had more adherent cells ( $140 \pm 11$  cells/mm<sup>2</sup> and  $1027 \pm 133$  cells/mm<sup>2</sup> after 3 days and 7 days) compared with untreated control Ti samples ( $116 \pm 20$  cells/mm<sup>2</sup> and  $828 \pm 90$  cells/mm<sup>2</sup> after 3 and 7 days).

As seen in **Fig. 18B** and **Fig. 19B**, Ti-FS+L control group exhibited blocking properties and minimum cell adhesion and proliferation was seen on these surfaces ( $56 \pm 11$  cells/mm<sup>2</sup>

and  $281 \pm 59$  cells/mm<sup>2</sup> after 3 and 7 days respectively). APTES75-TPFS25-collagen+L treated surfaces significantly increased cell proliferation and cell attachment when compared with control Ti-FS+L samples ( $P < 0.001$ ). Additionally, APTES75-TPFS25-collagen+L treated samples, GPTMS75-TPFS25-chitosan+L samples significantly increased cell viability and adhesion when compared with Ti-FS+L samples with  $P < 0.001$  and  $P < 0.01$ , respectively.

When comparing the results obtained from mixed silane modified surfaces with chitosan-DHB-FS+L modified samples from the previous experiments, cell attachment and proliferation significantly increased and biofunctionalized lubricant-infused surfaces created using the mixed silane approach showed better bioactivity and targeted cell adhesion properties (**Figures 17, 18 and 19**).

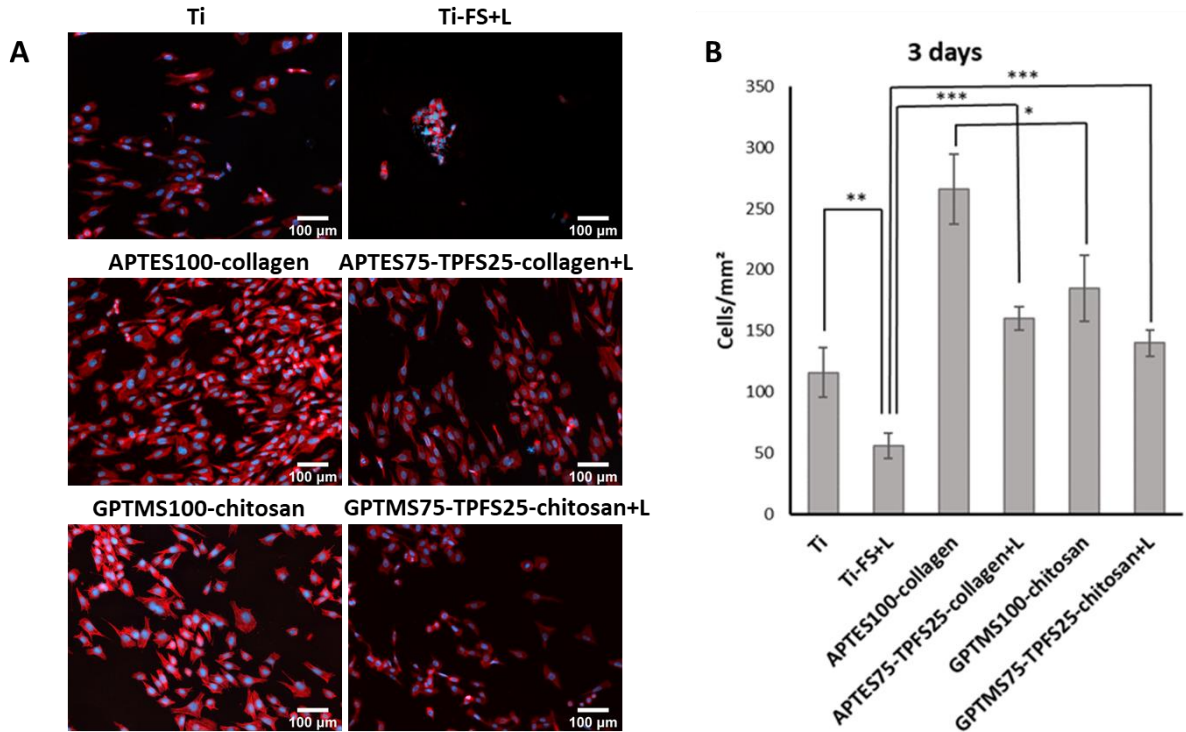


**Figure 18.** SaOS-2 cell proliferation after 3 days visualized by fluorescence microscopy (nuclei: blue; microfilaments: red) on the surface of control and experimental groups, **A)** Representative fluorescence images showing the density and distribution of adherent cells, **B)** Number of adherent cells on control and treated titanium after 3 days of cell culture. Error bars represent the SD of the mean of at least three samples. \*\*\*  $P < 0.001$ , \*\*  $P < 0.01$  and \*  $P < 0.05$  when compared with control samples.

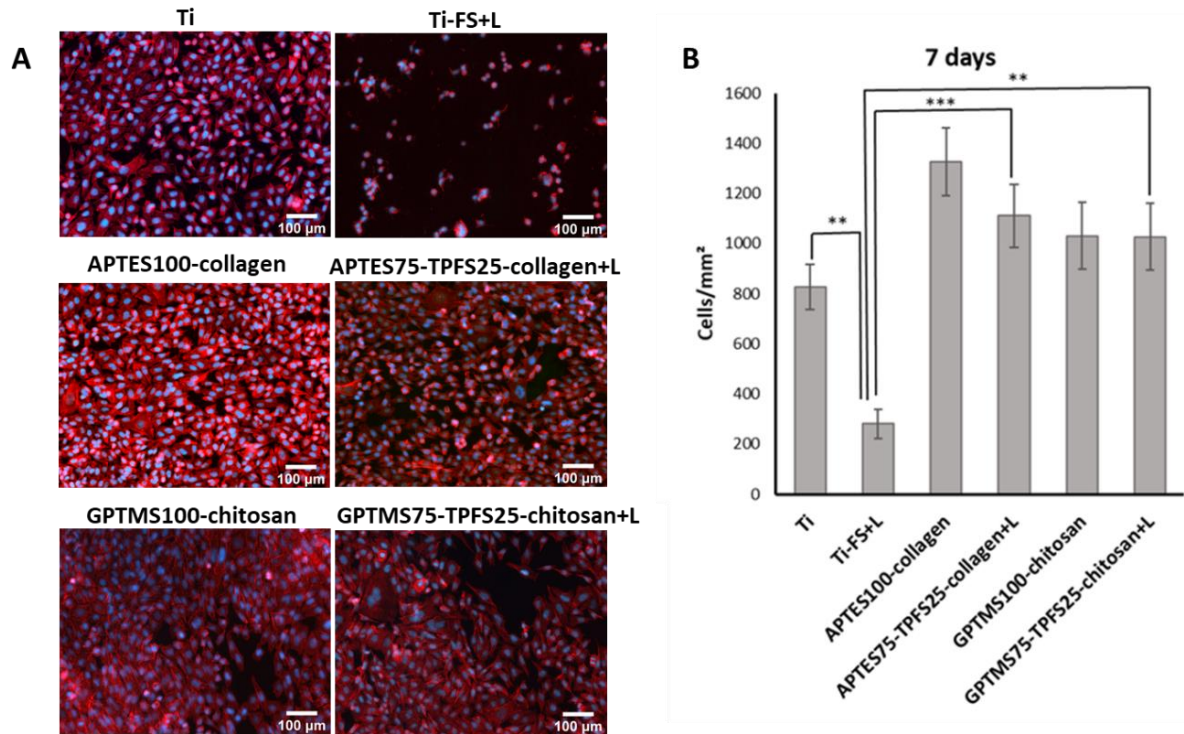


**Figure 19.** SaOS-2 cell proliferation after 7 days visualized by fluorescence microscopy (nuclei: blue; microfilaments: red) on the surface of control and experimental groups, **A**) Representative fluorescence images showing the density and distribution of adherent cells, **B**) Number of adherent cells on control and treated titanium after 3 and 7 days of cell culture. Error bars represent the SD of the mean of at least three samples. \*\*\*  $P < 0.001$  and \*\*  $P < 0.01$  when compared with control samples.

As illustrated in **Fig. 18** and **19**, cell adhesion was significantly higher in APTES100-collagen samples compared with GPTMS100-chitosan after 3 days ( $P < 0.05$ ), but there was no significant difference between these two groups after 7 days of culture.

Cell morphology was observed by immunofluorescence staining of cytoskeleton actin (**Figure 20**). SAOS-2 cells exhibit a spherical shape in the early stages of attachment and as time passes, actin filaments of cells will spread along two directions and an actin filament

network will form around the cell nucleus after 24 h of cultivation.<sup>148</sup> As seen in **Fig. 20**, APTES75-TPFS25-collagen+L and GPTMS75-TPFS25-chitosan+L samples promote cell attachment, and exhibit well cell spreading and protein expression which can be observed by the fluorescence images obtained after actin filament staining (red). Given the growth and differentiation of cells are accompanied with cytoskeleton, nuclei and actin of cells elongation, the filament network wrapped around the cell nucleus shows enhanced viability of cells.<sup>142</sup> In summary, bio-functional lubricant-infused titanium surfaces modified with mixed silanes and functionalized with collagen or chitosan improve surface biocompatibility and promote cells proliferation and growth. Additionally, APTES100-collagen coated surfaces significantly increased cell attachment compared with GPTMS100-chitosan coated surfaces in the first 3 days, but no significant difference was found after 7 days of cultivation. Although bioactivity is important for implant fixation and stability, preventing bacterial adhesion and infection are also important factors that lead to implant failure.<sup>4</sup> According to the result obtained from the biofilm experiments in **Fig. 15**, collagen lacks anti-bacterial properties which makes it an unsuitable candidate for titanium implants. Overall, when summarizing the results obtained from the biofilm formation studies and cell adhesion experiments performed on different coated titanium substrates, GPTMS75-TPFS25-chitosan+L group exhibited superior antibacterial and targeted cell binding properties compared with other coated surfaces and these surfaces are the optimal group for preparing biofunctionalized LIS on titanium implants.

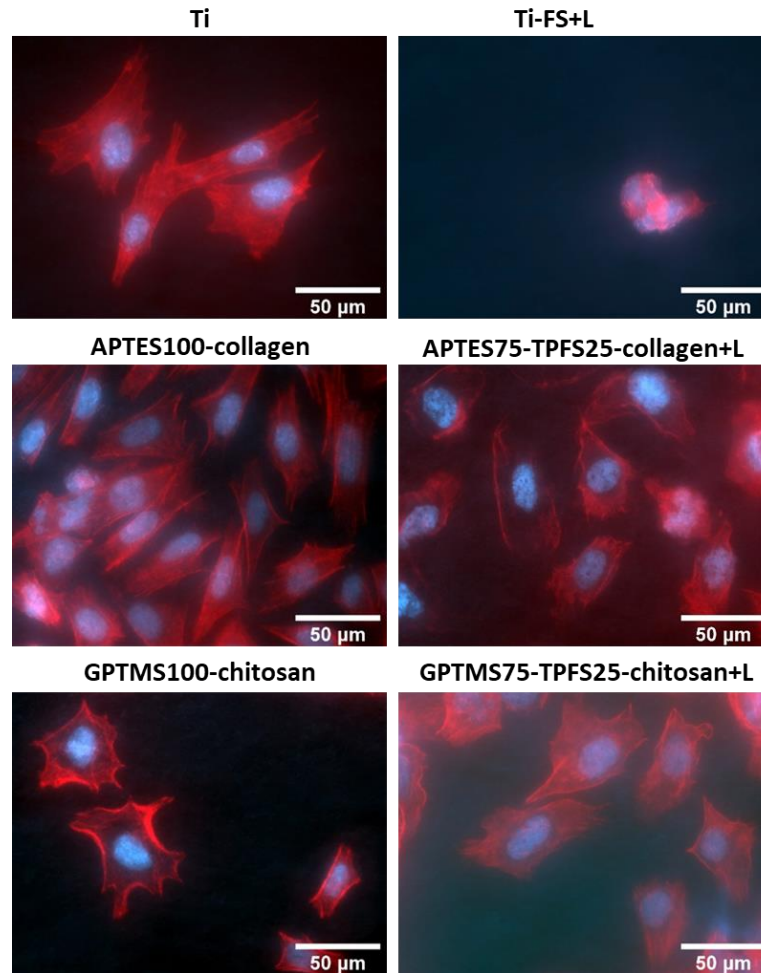


**Figure 20.** Immunofluorescence staining of nucleus and actin-based cytoskeleton (nuclei: blue; microfilaments: red) in human SAOS-2 cells to observe cell morphology after 7 days of cell culture.

## CHAPTER FIVE: CONCLUSION

In this thesis, we looked at the effect of using different surface modification methods to impregnate lubricant-infused surfaces with bio-functional features to enable titanium surfaces to exhibit simultaneous anti-biofouling and osseointegration properties. The performance of the titanium coated surfaces was examined by performing biofilm formation and cell culture experiments. Among different methods, titanium surfaces modified by mixed silanes showed great potential for obtaining a bio-functional lubricant-infused surface coating. In wettability measurements, titanium substrates modified by the CVD method using mixed silanes were able to lock-in the lubricant layer and form functional LIS. In cell culture experiments, both collagen and chitosan functionalized titanium substrates with LIS significantly enhanced cell attachment and proliferation. However, LIS titanium surfaces biofunctionalized with chitosan were able to block bacterial adhesion and prevent biofilm formation.

Based on the above analysis, LIS titanium surfaces biofunctionalized with chitosan using the mixed silane approach (GPTMS75-TPFS25-chitosan+L) is the optimized surface coating to combine both anti-biofouling and cell adhesion properties on titanium substrates. The designed surfaces coating could be applied to titanium implants for preventing biofilm formation and promoting targeted binding of cells.

The bio-functional and lubricant-infused surfaces could be applied in different titanium made medical implants such as knee joint prosthesis, acetabular and shoulder prosthesis<sup>149</sup>

as well as permanent implants made of other materials, like cobalt-chromium alloy,<sup>149</sup> carbon fiber<sup>150</sup> and aluminium oxide used in ceramic acetabular sockets<sup>151</sup>.

In future work, we need to do in vivo animal studies to confirm the results and explain the mechanism behind properties. Additionally, hyperglycaemia inhibits osteoblasts differentiation and it is proved in some research that diabetes can inhibit osseointegration and reduce bone-implant contact.<sup>152,153</sup> Diabetes plays negative effect in osteogenic signaling pathway and chitosan has potential in reactivating PI3K/AKT pathway under diabetic conditions.<sup>154</sup> This effect could be tested in diabetes model and compared with normal model.

## REFERENCE

- (1) Khorasani, A. M.; Goldberg, M.; Doeven, E. H.; Littlefair, G. Titanium in Biomedical Applications—Properties and Fabrication: A Review. *Journal of Biomaterials and Tissue Engineering*. American Scientific Publishers August 1, 2015, pp 593–619. <https://doi.org/10.1166/jbt.2015.1361>.
- (2) Sidambe, A. T. Biocompatibility of Advanced Manufactured Titanium Implants-A Review. *Materials*. MDPI AG 2014, pp 8168–8188. <https://doi.org/10.3390/ma7128168>.
- (3) Boehlert, C. J.; Cowen, C. J.; Quast, J. P.; Akahori, T.; Niinomi, M. Fatigue and Wear Evaluation of Ti-Al-Nb Alloys for Biomedical Applications. *Mater. Sci. Eng. C* **2008**, 28 (3), 323–330. <https://doi.org/10.1016/j.msec.2007.04.003>.
- (4) Sia, I. G.; Berbari, E. F.; Karchmer, A. W. Prosthetic Joint Infections. *Infectious Disease Clinics of North America*. Elsevier December 1, 2005, pp 885–914. <https://doi.org/10.1016/j.idc.2005.07.010>.
- (5) Kulkarni Aranya, A.; Pushalkar, S.; Zhao, M.; LeGeros, R. Z.; Zhang, Y.; Saxena, D. Antibacterial and Bioactive Coatings on Titanium Implant Surfaces. *J. Biomed. Mater. Res. A* **2017**, 105 (8), 2218–2227. <https://doi.org/10.1002/jbm.a.36081>.
- (6) *Hip and Knee Replacements in Canada, 2017–2018: Canadian Joint Replacement Registry Annual Report*; Ottawa, 2019.
- (7) Ribeiro, M.; Monteiro, F. J.; Ferraz, M. P. Infection of Orthopedic Implants with Emphasis on Bacterial Adhesion Process and Techniques Used in Studying Bacterial-Material Interactions. *Biomatter* **2012**, 2 (4), 176–194. <https://doi.org/10.4161/biom.22905>.
- (8) Khatoon, Z.; McTiernan, C. D.; Suuronen, E. J.; Mah, T. F.; Alarcon, E. I. Bacterial Biofilm Formation on Implantable Devices and Approaches to Its Treatment and

- Prevention. *Heliyon*. Elsevier Ltd December 1, 2018, pp 1–36. <https://doi.org/10.1016/j.heliyon.2018.e01067>.
- (9) Wang, L.; Cao, W.; Wang, X.; Li, P.; Zhou, J.; Zhang, G.; Li, X.; Xing, X. Biodegradable Silver-Loaded Polycation Modified Nanodiamonds/Polyurethane Scaffold with Improved Antibacterial and Mechanical Properties for Cartilage Tissue Repairing. *J. Mater. Sci. Mater. Med.* **2019**, *30* (4), 1–12. <https://doi.org/10.1007/s10856-019-6244-8>.
- (10) Alves, D.; Olívia Pereira, M. Mini-Review: Antimicrobial Peptides and Enzymes as Promising Candidates to Functionalize Biomaterial Surfaces. *Biofouling* **2014**, *30* (4), 483–499. <https://doi.org/10.1080/08927014.2014.889120>.
- (11) Lemire, J. A.; Harrison, J. J.; Turner, R. J. Antimicrobial Activity of Metals: Mechanisms, Molecular Targets and Applications. *Nature Reviews Microbiology*. Nature Publishing Group June 13, 2013, pp 371–384. <https://doi.org/10.1038/nrmicro3028>.
- (12) Hwang, B. J.; Lee, S. H. Study on Micro Fabricated Stainless Steel Surface to Anti-Biofouling Using Electrochemical Fabrication. *Micro and Nano Systems Letters*. Society of Micro and Nano Systems December 1, 2017, p 16. <https://doi.org/10.1186/s40486-017-0050-1>.
- (13) Sun, M.; Wu, Q.; Xu, J.; He, F.; Brown, A. P.; Ye, Y. Vapor-Based Grafting of Crosslinked Poly(N-Vinyl Pyrrolidone) Coatings with Tuned Hydrophilicity and Anti-Biofouling Properties. *J. Mater. Chem. B* **2016**, *4* (15), 2669–2678. <https://doi.org/10.1039/c6tb00076b>.
- (14) Hadjesfandiari, N.; Yu, K.; Mei, Y.; Kizhakkedathu, J. N. Polymer Brush-Based Approaches for the Development of Infection-Resistant Surfaces. *Journal of Materials Chemistry B*. Royal Society of Chemistry August 21, 2014, pp 4968–4978. <https://doi.org/10.1039/c4tb00550c>.

- (15) MacCallum, N.; Howell, C.; Kim, P.; Sun, D.; Friedlander, R.; Ranisau, J.; Ahanotu, O.; Lin, J. J.; Vena, A.; Hatton, B.; et al. Liquid-Infused Silicone As a Biofouling-Free Medical Material. *ACS Biomater. Sci. Eng.* **2015**, *1* (1), 43–51. <https://doi.org/10.1021/ab5000578>.
- (16) Narayana, P. S. V. V. S.; Srihari, P. S. V. V. Biofilm Resistant Surfaces and Coatings on Implants: A Review. In *Materials Today: Proceedings*; Elsevier Ltd, 2019; Vol. 18, pp 4847–4853. <https://doi.org/10.1016/j.matpr.2019.07.475>.
- (17) Stigter, M.; Bezemer, J.; De Groot, K.; Layrolle, P. Incorporation of Different Antibiotics into Carbonated Hydroxyapatite Coatings on Titanium Implants, Release and Antibiotic Efficacy. *J. Control. Release* **2004**, *99* (1), 127–137. <https://doi.org/10.1016/j.jconrel.2004.06.011>.
- (18) Huang, L.; Liu, X. H.; Zhang, X. H.; Tan, L.; Liu, C. J. A Highly Efficient Bactericidal Surface Based on the Co-Capture Function and Photodynamic Sterilization. *J. Mater. Chem. B* **2018**, *6* (42), 6831–6841. <https://doi.org/10.1039/c8tb02010h>.
- (19) Hajipour, M. J.; Fromm, K. M.; Akbar Ashkarran, A.; Jimenez de Aberasturi, D.; Larramendi, I. R. de; Rojo, T.; Serpooshan, V.; Parak, W. J.; Mahmoudi, M. Antibacterial Properties of Nanoparticles. *Trends in Biotechnology*. Elsevier Current Trends October 1, 2012, pp 499–511. <https://doi.org/10.1016/j.tibtech.2012.06.004>.
- (20) Desai, N. P.; Hubbell, J. A. *Surface Physical Interpenetrating Networks of Poly(Ethylene Terephthalate) and Poly(Ethylene Oxide) with Biomedical Applications*; 1992; Vol. 25. <https://doi.org/10.1021/ma00027a038>.
- (21) Such, G. K.; Johnston, A. P. R.; Caruso, F. Engineered Hydrogen-Bonded Polymer Multilayers: From Assembly to Biomedical Applications. *Chem. Soc. Rev.* **2011**, *40* (1), 19–29. <https://doi.org/10.1039/c0cs00001a>.
- (22) Park, G. E.; Pattison, M. A.; Park, K.; Webster, T. J. Accelerated Chondrocyte

- Functions on NaOH-Treated PLGA Scaffolds. *Biomaterials* **2005**, 26 (16), 3075–3082. <https://doi.org/10.1016/j.biomaterials.2004.08.005>.
- (23) Davila, J.; Harriman, A. PHOTSENSITIZED OXIDATION OF BIOMATERIALS and RELATED MODEL COMPOUNDS. *Photochem. Photobiol.* **1989**, 50 (1), 29–35. <https://doi.org/10.1111/j.1751-1097.1989.tb04126.x>.
- (24) Gabriel, M.; Van Nieuw Amerongen, G. P.; Van Hinsbergh, V. W. M.; Van Nieuw Amerongen, A. V.; Zentner, A. Direct Grafting of RGD-Motif-Containing Peptide on the Surface of Polycaprolactone Films. *J. Biomater. Sci. Polym. Ed.* **2006**, 17 (5), 567–577. <https://doi.org/10.1163/156856206776986288>.
- (25) Back, D. A.; Bormann, N.; Calafi, A.; Zech, J.; Garbe, L. A.; Müller, M.; Willy, C.; Schmidmaier, G.; Wildemann, B. Testing of Antibiotic Releasing Implant Coatings to Fight Bacteria in Combat-Associated Osteomyelitis – an in-Vitro Study. *Int. Orthop.* **2016**, 40 (5), 1039–1047. <https://doi.org/10.1007/s00264-016-3142-2>.
- (26) Orapiriyakul, W.; Young, P. S.; Damiati, L.; Tsimbouri, P. M. Antibacterial Surface Modification of Titanium Implants in Orthopaedics. *J. Tissue Eng.* **2018**, 9. <https://doi.org/10.1177/2041731418789838>.
- (27) Movaffagh, J.; Ghodsi, A.; Bazzaz, B. S. F.; Tabassi, S. A. S.; Azadi, H. G. The Use of Natural Biopolymer of Chitosan as Biodegradable Beads for Local Antibiotic Delivery: Release Studies. *Jundishapur J. Nat. Pharm. Prod.* **2013**, 8 (1), 27–33. <https://doi.org/10.5812/jjnpp.7532>.
- (28) Benea, L.; Celis, J. P. Reactivity of Porous Titanium Oxide Film and Chitosan Layer Electrochemically Formed on Ti-6Al-4V Alloy in Biological Solution. *Surf. Coatings Technol.* **2018**, 354, 145–152. <https://doi.org/10.1016/J.SURFCOAT.2018.09.015>.
- (29) Gomes, A. P.; Mano, J. F.; Queiroz, J. A.; Gouveia, I. C. Layer-by-Layer Deposition of Antimicrobial Polymers on Cellulosic Fibers: A New Strategy to Develop

- Bioactive Textiles. *Polym. Adv. Technol.* **2013**, *24* (11), 1005–1010.  
<https://doi.org/10.1002/pat.3176>.
- (30) Costa-Pinto, A. R.; Reis, R. L.; Neves, N. M. Scaffolds Based Bone Tissue Engineering: The Role of Chitosan. *Tissue Eng. - Part B Rev.* **2011**, *17* (5), 331–347.  
<https://doi.org/10.1089/ten.teb.2010.0704>.
- (31) Moutzouri, A. G.; Athanassiou, G. M. Insights into the Alteration of Osteoblast Mechanical Properties upon Adhesion on Chitosan. *Biomed Res. Int.* **2014**, *2014* (6), 1–8. <https://doi.org/10.1155/2014/740726>.
- (32) Wang, Y.; Zhang, M.; Lai, Y.; Chi, L. Advanced Colloidal Lithography: From Patterning to Applications. *Nano Today*. Elsevier B.V. October 1, 2018, pp 36–61.  
<https://doi.org/10.1016/j.nantod.2018.08.010>.
- (33) Vasilev, K.; Griesser, S. S.; Griesser, H. J. Antibacterial Surfaces and Coatings Produced by Plasma Techniques. *Plasma Processes and Polymers*. John Wiley & Sons, Ltd November 23, 2011, pp 1010–1023.  
<https://doi.org/10.1002/ppap.201100097>.
- (34) Tsimbouri, P. M.; Fisher, L.; Holloway, N.; Sjostrom, T.; Nobbs, A. H.; Meek, R. M. D.; Su, B.; Dalby, M. J. Osteogenic and Bactericidal Surfaces from Hydrothermal Titania Nanowires on Titanium Substrates. *Sci. Rep.* **2016**, *6* (1), 1–12.  
<https://doi.org/10.1038/srep36857>.
- (35) Lasagni, A.; D'Alessandria, M.; Giovanelli, R.; Mücklich, F. Advanced Design of Periodical Architectures in Bulk Metals by Means of Laser Interference Metallurgy. *Appl. Surf. Sci.* **2007**, *254* (4), 930–936.  
<https://doi.org/10.1016/j.apsusc.2007.08.010>.
- (36) Chi, G. J.; Yao, S. W.; Fan, J.; Zhang, W. G.; Wang, H. Z. Antibacterial Activity of Anodized Aluminum with Deposited Silver. *Surf. Coatings Technol.* **2002**, *157* (2–3), 162–165. [https://doi.org/10.1016/S0257-8972\(02\)00150-0](https://doi.org/10.1016/S0257-8972(02)00150-0).

- (37) Watson, G. S.; Green, D. W.; Schwarzkopf, L.; Li, X.; Cribb, B. W.; Myhra, S.; Watson, J. A. A Gecko Skin Micro/Nano Structure - A Low Adhesion, Superhydrophobic, Anti-Wetting, Self-Cleaning, Biocompatible, Antibacterial Surface. *Acta Biomater.* **2015**, *21*, 109–122. <https://doi.org/10.1016/j.actbio.2015.03.007>.
- (38) Kelleher, S. M.; Habimana, O.; Lawler, J.; O'reilly, B.; Daniels, S.; Casey, E.; Cowley, A. Cicada Wing Surface Topography: An Investigation into the Bactericidal Properties of Nanostructural Features. *ACS Appl. Mater. Interfaces* **2016**, *8* (24), 14966–14974. <https://doi.org/10.1021/acsami.5b08309>.
- (39) Bixler, G. D.; Bhushan, B. Fluid Drag Reduction and Efficient Self-Cleaning with Rice Leaf and Butterfly Wing Bioinspired Surfaces. *Nanoscale*. Royal Society of Chemistry September 7, 2013, pp 7685–7710. <https://doi.org/10.1039/c3nr01710a>.
- (40) Yang, X.; Huang, Y.; Zhao, Y.; Zhang, X.; Wang, J.; Sann, E. E.; Mon, K. H.; Lou, X.; Xia, F. Bioinspired Slippery Lubricant-Infused Surfaces With External Stimuli Responsive Wettability: A Mini Review. *Front. Chem.* **2019**, *7*, 826. <https://doi.org/10.3389/fchem.2019.00826>.
- (41) Wang, D.; Guo, Z.; Liu, W. Bioinspired Edible Lubricant-Infused Surface with Liquid Residue Reduction Properties. *Research* **2019**, *2019*, 1–12. <https://doi.org/10.34133/2019/1649427>.
- (42) Zhang, P.; Chen, H.; Zhang, L.; Zhang, D. Anti-Adhesion Effects of Liquid-Infused Textured Surfaces on High-Temperature Stainless Steel for Soft Tissue. *Appl. Surf. Sci.* **2016**, *385*, 249–256. <https://doi.org/10.1016/j.apsusc.2016.05.110>.
- (43) Doll, K.; Fadeeva, E.; Schaeske, J.; Ehmke, T.; Winkel, A.; Heisterkamp, A.; Chichkov, B. N.; Stiesch, M.; Stumpp, N. S. Development of Laser-Structured Liquid-Infused Titanium with Strong Biofilm-Repellent Properties. *ACS Appl. Mater. Interfaces* **2017**, *9* (11), 9359–9368. <https://doi.org/10.1021/acsami.6b16159>.

- (44) Badv, M.; Jaffer, I. H.; Weitz, J. I.; Didar, T. F. An Omniphobic Lubricant-Infused Coating Produced by Chemical Vapor Deposition of Hydrophobic Organosilanes Attenuates Clotting on Catheter Surfaces. *Sci. Rep.* **2017**, *7* (1), 11639. <https://doi.org/10.1038/s41598-017-12149-1>.
- (45) Epstein, A. K.; Wong, T.-S.; Belisle, R. A.; Boggs, E. M.; Aizenberg, J. Liquid-Infused Structured Surfaces with Exceptional Anti-Biofouling Performance. *Proc. Natl. Acad. Sci. U. S. A.* **2012**, *109* (33), 13182–13187. <https://doi.org/10.1073/pnas.1201973109>.
- (46) Kratochvil, M. J.; Welsh, M. A.; Manna, U.; Ortiz, B. J.; Blackwell, H. E.; Lynn, D. M. Slippery Liquid-Infused Porous Surfaces That Prevent Bacterial Surface Fouling and Inhibit Virulence Phenotypes in Surrounding Planktonic Cells. *ACS Infect. Dis.* **2016**, *2* (7), 509–517. <https://doi.org/10.1021/acsinfecdis.6b00065>.
- (47) Villegas, M.; Zhang, Y.; Abu Jarad, N.; Soleymani, L.; Didar, T. F. Liquid-Infused Surfaces: A Review of Theory, Design, and Applications. *ACS Nano* **2019**, *13* (8), 8517–8536. <https://doi.org/10.1021/acsnano.9b04129>.
- (48) Abe, J.; Tenjimabayashi, M.; Shiratori, S. Electrospun Nanofiber SLIPS Exhibiting High Total Transparency and Scattering. *RSC Adv.* **2016**, *6* (44), 38018–38023. <https://doi.org/10.1039/c6ra00276e>.
- (49) Sunny, S.; Vogel, N.; Howell, C.; Vu, T. L.; Aizenberg, J. Lubricant-Infused Nanoparticulate Coatings Assembled by Layer-by-Layer Deposition. *Adv. Funct. Mater.* **2014**, *24* (42), 6658–6667. <https://doi.org/10.1002/adfm.201401289>.
- (50) Ma, W.; Higaki, Y.; Otsuka, H.; Takahara, A. Perfluoropolyether-Infused Nano-Texture: A Versatile Approach to Omniphobic Coatings with Low Hysteresis and High Transparency. *Chem. Commun.* **2013**, *49* (6), 597–599. <https://doi.org/10.1039/c2cc37576a>.
- (51) Ware, C. S.; Smith-Palmer, T.; Peppou-Chapman, S.; Scarratt, L. R. J.; Humphries,

- E. M.; Balzer, D.; Neto, C. Marine Antifouling Behavior of Lubricant-Infused Nanowrinkled Polymeric Surfaces. *ACS Appl. Mater. Interfaces* **2018**, *10* (4), 4173–4182. <https://doi.org/10.1021/acsami.7b14736>.
- (52) Yang, J.; Song, H.; Ji, H.; Chen, B. Slippery Lubricant-Infused Textured Aluminum Surfaces. *J. Adhes. Sci. Technol.* **2014**, *28* (19), 1949–1957. <https://doi.org/10.1080/01694243.2014.933563>.
- (53) Zhang, F.; Sautter, K.; Larsen, A. M.; Findley, D. A.; Davis, R. C.; Samha, H.; Linford, M. R. Chemical Vapor Deposition of Three Aminosilanes on Silicon Dioxide: Surface Characterization, Stability, Effects of Silane Concentration, and Cyanine Dye Adsorption. *Langmuir* **2010**, *26* (18), 14648–14654. <https://doi.org/10.1021/la102447y>.
- (54) Liu, Z. Z.; Wang, Q.; Liu, X.; Bao, J. Q. Effects of Amino-Terminated Self-Assembled Monolayers on Nucleation and Growth of Chemical Vapor-Deposited Copper Films. *Thin Solid Films* **2008**, *517* (2), 635–640. <https://doi.org/10.1016/j.tsf.2008.07.030>.
- (55) Wong, T.-S.; Kang, S. H.; Tang, S. K. Y.; Smythe, E. J.; Hatton, B. D.; Grinthal, A.; Aizenberg, J. Bioinspired Self-Repairing Slippery Surfaces with Pressure-Stable Omniphobicity. *Nature* **2011**, *477* (7365), 443–447. <https://doi.org/10.1038/nature10447>.
- (56) Bhattacharyya, B.; Doloi, B. Micromachining Processes. In *Modern Machining Technology*; Elsevier, 2020; pp 593–673. <https://doi.org/10.1016/b978-0-12-812894-7.00007-4>.
- (57) Hagberg, K.; Brånemark, R. One Hundred Patients Treated with Osseointegrated Transfemoral Amputation Prostheses - Rehabilitation Perspective. *J. Rehabil. Res. Dev.* **2009**, *46* (3), 331–344. <https://doi.org/10.1682/JRRD.2008.06.0080>.
- (58) Scholz, I.; Bückins, M.; Dolge, L.; Erlinghagen, T.; Weth, A.; Hischen, F.; Mayer,

- J.; Hoffmann, S.; Riederer, M.; Riedel, M.; et al. Slippery Surfaces of Pitcher Plants: Nepenthes Wax Crystals Minimize Insect Attachment via Microscopic Surface Roughness. *J. Exp. Biol.* **2010**, *213* (7), 1115–1125. <https://doi.org/10.1242/jeb.035618>.
- (59) Wong, T. S.; Kang, S. H.; Tang, S. K. Y.; Smythe, E. J.; Hatton, B. D.; Grinthal, A.; Aizenberg, J. Bioinspired Self-Repairing Slippery Surfaces with Pressure-Stable Omniphobicity. *Nature* **2011**, *477* (7365), 443–447. <https://doi.org/10.1038/nature10447>.
- (60) Smith, J. D.; Dhiman, R.; Anand, S.; Reza-Garduno, E.; Cohen, R. E.; McKinley, G. H.; Varanasi, K. K. Droplet Mobility on Lubricant-Impregnated Surfaces. *Soft Matter* **2013**, *9* (6), 1772–1780. <https://doi.org/10.1039/C2SM27032C>.
- (61) Smith, J. D.; Dhiman, R.; Anand, S.; Reza-Garduno, E.; Cohen, R. E.; McKinley, G. H.; Varanasi, K. K. Droplet Mobility on Lubricant-Impregnated Surfaces. *Soft Matter* **2013**, *9* (6), 1772–1780. <https://doi.org/10.1039/c2sm27032c>.
- (62) Schellenberger, F.; Xie, J.; Encinas, N.; Hardy, A.; Klapper, M.; Papadopoulos, P.; Butt, H.-J.; Vollmer, D. Direct Observation of Drops on Slippery Lubricant-Infused Surfaces. *Soft Matter* **2015**, *11* (38), 7617–7626. <https://doi.org/10.1039/C5SM01809A>.
- (63) Preston, D. J.; Song, Y.; Lu, Z.; Antao, D. S.; Wang, E. N. Design of Lubricant Infused Surfaces. <https://doi.org/10.1021/acsami.7b14311>.
- (64) Howell, C.; Grinthal, A.; Sunny, S.; Aizenberg, M.; Aizenberg, J. Designing Liquid-Infused Surfaces for Medical Applications: A Review. *Advanced Materials*. Wiley-VCH Verlag December 13, 2018, p 1802724. <https://doi.org/10.1002/adma.201802724>.
- (65) Zhang, P.; Chen, H.; Li, L.; Liu, H.; Liu, G.; Zhang, L.; Zhang, D.; Jiang, L. Bioinspired Smart Peristome Surface for Temperature-Controlled Unidirectional

- Water Spreading. *ACS Appl. Mater. Interfaces* **2017**, *9* (6), 5645–5652. <https://doi.org/10.1021/acsami.6b15802>.
- (66) Qian, H.; Zhang, D.; Deng, L.; Huang, L.; Xu, D.; Du, C.; Li, X. The Role of Surface Morphology in the Barrier Properties of Epoxy Coatings in Different Corrosion Environments. *Prog. Org. Coatings* **2017**, *104*, 199–209. <https://doi.org/10.1016/j.porgcoat.2016.11.002>.
- (67) Doll, K.; Fadeeva, E.; Schaeske, J.; Ehmke, T.; Winkel, A.; Heisterkamp, A.; Chichkov, B. N.; Stiesch, M.; Stumpp, N. S. Development of Laser-Structured Liquid-Infused Titanium with Strong Biofilm-Repellent Properties. *ACS Appl. Mater. Interfaces* **2017**, *9* (11), 9359–9368. <https://doi.org/10.1021/acsami.6b16159>.
- (68) Bazyar, H.; Van De Beek, N.; Lammertink, R. G. H. Liquid-Infused Membranes with Oil-in-Water Emulsions. *Langmuir* **2019**, *35* (29), 9513–9520. <https://doi.org/10.1021/acs.langmuir.9b01055>.
- (69) TAS, M.; Memon, H.; Xu, F.; Ahmed, I.; Hou, X. Electrospun Nanofibre Membrane Based Transparent Slippery Liquid-Infused Porous Surfaces with Icephobic Properties. *Colloids Surfaces A Physicochem. Eng. Asp.* **2020**, *585*, 124177. <https://doi.org/10.1016/j.colsurfa.2019.124177>.
- (70) Ujjain, S. K.; Roy, P. K.; Kumar, S.; Singha, S.; Khare, K. Uniting Superhydrophobic, Superoleophobic and Lubricant Infused Slippery Behavior on Copper Oxide Nano-Structured Substrates. *Sci. Rep.* **2016**, *6*. <https://doi.org/10.1038/srep35524>.
- (71) Villegas, M.; Zhang, Y.; Abu Jarad, N.; Soleymani, L.; Didar, T. F. Liquid-Infused Surfaces: A Review of Theory, Design, and Applications. *ACS Nano* **2019**, *13* (8), 8517–8536. <https://doi.org/10.1021/acs.nano.9b04129>.
- (72) Zhu, G. H.; Cho, S. H.; Zhang, H.; Zhao, M.; Zacharia, N. S. Slippery Liquid-Infused Porous Surfaces (SLIPS) Using Layer-by-Layer Polyelectrolyte Assembly in

- Organic Solvent. *Langmuir* **2018**, *34* (16), 4722–4731. <https://doi.org/10.1021/acs.langmuir.8b00335>.
- (73) Badv, M.; Jaffer, I. H.; Weitz, J. I.; Didar, T. F. An Omniphobic Lubricant-Infused Coating Produced by Chemical Vapor Deposition of Hydrophobic Organosilanes Attenuates Clotting on Catheter Surfaces. *Sci. Rep.* **2017**, *7* (1), 11639. <https://doi.org/10.1038/s41598-017-12149-1>.
- (74) Badv, M.; Imani, S. M.; Weitz, J. I.; Didar, T. F. Lubricant-Infused Surfaces with Built-In Functional Biomolecules Exhibit Simultaneous Repellency and Tunable Cell Adhesion. *ACS Nano* **2018**, *12* (11), 10890–10902. <https://doi.org/10.1021/acsnano.8b03938>.
- (75) Ashrafi, Z.; Lucia, L.; Krause, W. Nature-Inspired Liquid Infused Systems for Superwetable Surface Energies. *ACS Applied Materials and Interfaces*. American Chemical Society June 19, 2019, pp 21275–21293. <https://doi.org/10.1021/acsami.9b00930>.
- (76) Jayesh, R. S.; Dhinakarsamy, V. Osseointegration. *Journal of Pharmacy and Bioallied Sciences*. Medknow Publications April 1, 2015, pp S226–S229. <https://doi.org/10.4103/0975-7406.155917>.
- (77) Jin, W.; Chu, P. K. Orthopedic Implants. In *Encyclopedia of Biomedical Engineering*; Elsevier, 2018; Vol. 1–3, pp 425–439. <https://doi.org/10.1016/B978-0-12-801238-3.10999-7>.
- (78) Petersen, R. Titanium Implant Osseointegration Problems with Alternate Solutions Using Epoxy/Carbon-Fiber-Reinforced Composite. *Metals (Basel)*. **2014**, *4* (4), 549–569. <https://doi.org/10.3390/met4040549>.
- (79) Smeets, R.; Stadlinger, B.; Schwarz, F.; Beck-Broichsitter, B.; Jung, O.; Precht, C.; Kloss, F.; Gröbe, A.; Heiland, M.; Ebker, T. Impact of Dental Implant Surface Modifications on Osseointegration. *BioMed Research International*. Hindawi

- Limited 2016, pp 1–16. <https://doi.org/10.1155/2016/6285620>.
- (80) Y., A.; Valds-Flores, M.; Orozco, L.; Velzquez-Cruz, R. Molecular Aspects of Bone Remodeling. In *Topics in Osteoporosis*; InTech, 2013; pp 1–27. <https://doi.org/10.5772/54905>.
- (81) Florencio-Silva, R.; Rodrigues Da, G.; Sasso, S.; Sasso-Cerri, E.; Simões, M. J.; Cerri, P. S. Biology of Bone Tissue: Structure, Function, and Factors That Influence Bone Cells. **2015**. <https://doi.org/10.1155/2015/421746>.
- (82) Stewart, C.; Akhavan, B.; Wise, S. G.; Bilek, M. M. M. A Review of Biomimetic Surface Functionalization for Bone-Integrating Orthopedic Implants: Mechanisms, Current Approaches, and Future Directions. *Progress in Materials Science*. Elsevier Ltd December 1, 2019, p 100588. <https://doi.org/10.1016/j.pmatsci.2019.100588>.
- (83) Gittens, R. A.; Scheideler, L.; Rupp, F.; Hyzy, S. L.; Geis-Gerstorfer, J.; Schwartz, Z.; Boyan, B. D. A Review on the Wettability of Dental Implant Surfaces II: Biological and Clinical Aspects. *Acta Biomaterialia*. Elsevier Ltd 2014, pp 2907–2918. <https://doi.org/10.1016/j.actbio.2014.03.032>.
- (84) Korotin, D. M.; Bartkowski, S.; Kurmaev, E. Z.; Meumann, M.; Yakushina, E. B.; Valiev, R. Z.; Cholakh, S. O. Surface Characterization of Titanium Implants Treated in Hydrofluoric Acid. *J. Biomater. Nanobiotechnol.* **2012**, *03* (01), 87–91. <https://doi.org/10.4236/jbnb.2012.31011>.
- (85) Ivanoff, C. J.; Hallgren, C.; Widmark, G.; Sennerby, L.; Wennerberg, A. Histologic Evaluation of the Bone Integration of TiO<sub>2</sub> Blasted and Turned Titanium Microimplants in Humans. *Clin. Oral Implants Res.* **2001**, *12* (2), 128–134. <https://doi.org/10.1034/j.1600-0501.2001.012002128.x>.
- (86) Jia, S.; Zhang, Y.; Ma, T.; Chen, H.; Lin, Y. Enhanced Hydrophilicity and Protein Adsorption of Titanium Surface by Sodium Bicarbonate Solution. *J. Nanomater.* **2015**, *2015*, 1–12. <https://doi.org/10.1155/2015/536801>.

- (87) Buser, D.; Brogini, N.; Wieland, M.; Schenk, R. K.; Denzer, A. J.; Cochran, D. L.; Hoffmann, B.; Lussi, A.; Steinemann, S. G. Enhanced Bone Apposition to a Chemically Modified SLA Titanium Surface. *J. Dent. Res.* **2004**, *83* (7), 529–533. <https://doi.org/10.1177/154405910408300704>.
- (88) Allegrini Jr, S.; Yoshimoto, M.; Barbosa Salles, M.; de Almeida Bressiani, A. H. Biologic Response to Titanium Implants with Laser-Treated Surfaces. *Int. J. Oral Maxillofac. Implants* **2014**, *29* (1), 63–70. <https://doi.org/10.11607/jomi.3213>.
- (89) Larsson Wexell, C.; Shah, F. A.; Ericson, L.; Matic, A.; Palmquist, A.; Thomsen, P. Electropolished Titanium Implants with a Mirror-Like Surface Support Osseointegration and Bone Remodelling. **2016**. <https://doi.org/10.1155/2016/1750105>.
- (90) Smirnov, I. V.; Rau, J. V.; Fosca, M.; de Bonis, A.; Latini, A.; Teghil, R.; Kalita, V. I.; Fedotov, A. Y.; Gudkov, S. V.; Baranchikov, A. E.; et al. Structural Modification of Titanium Surface by Octacalcium Phosphate via Pulsed Laser Deposition and Chemical Treatment. *Bioact. Mater.* **2017**, *2* (2), 101–107. <https://doi.org/10.1016/j.bioactmat.2017.03.002>.
- (91) Bai, Y.; Zhou, R.; Cao, J.; Wei, D.; Du, Q.; Li, B.; Wang, Y.; Jia, D.; Zhou, Y. Microarc Oxidation Coating Covered Ti Implants with Micro-Scale Gouges Formed by a Multi-Step Treatment for Improving Osseointegration. *Mater. Sci. Eng. C* **2017**, *76*, 908–917. <https://doi.org/10.1016/j.msec.2017.03.071>.
- (92) Mao, Y.; Li, X. Research Progress on the Biochemical Modification of Titanium Implant Surface. *Med chem, an open access J.* **2014**, *4* (11), 742–747. <https://doi.org/10.4172/2161-0444.1000224>.
- (93) Stylianou, A.; Yova, D.; Politopoulos, K. Atomic Force Microscopy Surface Nanocharacterization of UV-Irradiated Collagen Thin Films. In *IEEE 12th International Conference on BioInformatics and BioEngineering, BIBE 2012*; 2012;

- pp 602–607. <https://doi.org/10.1109/BIBE.2012.6399741>.
- (94) Simina Corobea, M.; Albu, G.; Ion, R.; Cimpean, A.; Miculescu, F.; Antoniac, V.; Raditoiu, V.; Sirbu, I.; Stoenescu, M.; Ioan, S.; et al. Modification of Titanium Surface with Collagen and Doxycycline as a New Approach in Dental Implants. **2015**. <https://doi.org/10.1080/01694243.2015.1073661>.
- (95) Haimov, H.; Yosupov, N.; Pinchasov, G.; Juodzbalys, G. Bone Morphogenetic Protein Coating on Titanium Implant Surface: A Systematic Review. *J. Oral Maxillofac. Res.* **2017**, 8 (2). <https://doi.org/10.5037/jomr.2017.8201>.
- (96) Strauss, F. J.; Di Summa, F.; Stähli, A.; Matos, L.; Vaca, F.; Schuldt, G.; Gruber, R. TGF- $\beta$  Activity in Acid Bone Lysate Adsorbs to Titanium Surface. *Clin. Implant Dent. Relat. Res.* **2019**, 21 (2), 336–343. <https://doi.org/10.1111/cid.12734>.
- (97) Lynch, S. E.; Buser, D.; Hernandez, R. A.; Weber, H. P.; Stich, H.; Fox, C. H.; Williams, R. C. Effects of the Platelet-Derived Growth Factor/Insulin-Like Growth Factor-I Combination on Bone Regeneration Around Titanium Dental Implants. Results of a Pilot Study in Beagle Dogs. *J. Periodontol.* **1991**, 62 (11), 710–716. <https://doi.org/10.1902/jop.1991.62.11.710>.
- (98) López-Quiles, J.; Forteza-López, A.; Montiel, M.; Clemente, C.; Fernández-Tresguerres, J. Á.; Fernández-Tresguerres, I. Effects of Locally Applied Insulin-like Growth Factor-i on Osseointegration. *Med. Oral Patol. Oral y Cir. Bucal* **2019**, 24 (5), e652–e658. <https://doi.org/10.4317/medoral.22973>.
- (99) Nelson Elias, C.; Abdo Gravina, P.; Silva Filho, C.; Augusto de Paula Nascente, P. Preparation of Bioactive Titanium Surfaces via Fluoride and Fibronectin Retention. *Int. J. Biomater.* **2012**, 2012. <https://doi.org/10.1155/2012/290179>.
- (100) Park, J.-M.; Koak, J.-Y.; Jang, J.-H.; Han, C.-H.; Kim, S.-K.; Heo, S.-J. Osseointegration of Anodized Titanium Implants Coated with Fibroblast Growth Factor-Fibronectin (FGF-FN) Fusion Protein. *Int. J. Oral Maxillofac. Implants* **2006**,

21 (6), 859–866.

- (101) Liu, Y.; Enggist, L.; Kuffer, A. F.; Buser, D.; Hunziker, E. B. The Influence of BMP-2 and Its Mode of Delivery on the Osteoconductivity of Implant Surfaces during the Early Phase of Osseointegration. *Biomaterials* **2007**, *28* (16), 2677–2686. <https://doi.org/10.1016/j.biomaterials.2007.02.003>.
- (102) Liu, W.; Merrett, K.; Griffith, M.; Fagerholm, P.; Dravida, S.; Heyne, B.; Scaiano, J. C.; Watsky, M. A.; Shinozaki, N.; Lagali, N.; et al. Recombinant Human Collagen for Tissue Engineered Corneal Substitutes. *Biomaterials* **2008**, *29* (9), 1147–1158. <https://doi.org/10.1016/j.biomaterials.2007.11.011>.
- (103) Dupont, K. M.; Boerckel, J. D.; Stevens, H. Y.; Diab, T.; Kolambkar, Y. M.; Takahata, M.; Schwarz, E. M.; Guldberg, R. E. Synthetic Scaffold Coating with Adeno-Associated Virus Encoding BMP2 to Promote Endogenous Bone Repair. *Cell Tissue Res.* **2012**, *347* (3), 575–588. <https://doi.org/10.1007/s00441-011-1197-3>.
- (104) van den Beucken, J. J. J. P.; Walboomers, X. F.; Leeuwenburgh, S. C. G.; Vos, M. R. J.; Sommerdijk, N. A. J. M.; Nolte, R. J. M.; Jansen, J. A. Multilayered DNA Coatings: In Vitro Bioactivity Studies and Effects on Osteoblast-like Cell Behavior. *Acta Biomater.* **2007**, *3* (4), 587–596. <https://doi.org/10.1016/j.actbio.2006.12.007>.
- (105) Sakurai, T.; Yoshinari, M.; Toyama, T.; Hayakawa, T.; Ohkubo, C. Effects of a Multilayered DNA/Protamine Coating on Titanium Implants on Bone Responses. *J. Biomed. Mater. Res. Part A* **2016**, *104* (6), 1500–1509. <https://doi.org/10.1002/jbm.a.35679>.
- (106) Venkatesan, J.; Kim, S.-K. Chitosan Composites for Bone Tissue Engineering--an Overview. *Mar. Drugs* **2010**, *8* (8), 2252–2266. <https://doi.org/10.3390/md8082252>.
- (107) Bumgardner, J. D.; Wisner, R.; Elder, S. H.; Jouett, R.; Yang, Y.; Ong, J. L. Contact Angle, Protein Adsorption and Osteoblast Precursor Cell Attachment to Chitosan

- Coatings Bonded to Titanium. *J. Biomater. Sci. Polym. Ed.* **2003**, *14* (12), 1401–1409. <https://doi.org/10.1163/156856203322599734>.
- (108) Bumgardner, J. D.; Wiser, R.; Gerard, P. D.; Bergin, P.; Chestnutt, B.; Marini, M.; Ramsey, V.; Elder, S. H.; Gilbert, J. A. Chitosan: Potential Use as a Bioactive Coating for Orthopaedic and Craniofacial/Dental Implants. *J. Biomater. Sci. Polym. Ed.* **2003**, *14* (5), 423–438. <https://doi.org/10.1163/156856203766652048>.
- (109) Lahiji, A.; Sohrabi, A.; Hungerford, D. S.; Frondoza, C. G. Chitosan Supports the Expression of Extracellular Matrix Proteins in Human Osteoblasts and Chondrocytes. *J. Biomed. Mater. Res.* **2000**, *51* (4), 586–595. [https://doi.org/10.1002/1097-4636\(20000915\)51:4<586::aid-jbm6>3.0.co;2-s](https://doi.org/10.1002/1097-4636(20000915)51:4<586::aid-jbm6>3.0.co;2-s).
- (110) Renoud, P.; Toury, B.; Benayoun, S.; Attik, G.; Grosgeat, B. Functionalization of Titanium with Chitosan via Silanation: Evaluation of Biological and Mechanical Performances. *PLoS One* **2012**, *7* (7), 39367. <https://doi.org/10.1371/journal.pone.0039367>.
- (111) Arciola, C. R.; Campoccia, D.; Speziale, P.; Montanaro, L.; Costerton, J. W. Biofilm Formation in Staphylococcus Implant Infections. A Review of Molecular Mechanisms and Implications for Biofilm-Resistant Materials. *Biomaterials*. September 2012, pp 5967–5982. <https://doi.org/10.1016/j.biomaterials.2012.05.031>.
- (112) Li, X.; Ma, X.-Y.; Feng, Y.-F.; Ma, Z.-S.; Wang, J.; Ma, T.-C.; Qi, W.; Lei, W.; Wang, L. Osseointegration of Chitosan Coated Porous Titanium Alloy Implant by Reactive Oxygen Species-Mediated Activation of the PI3K/AKT Pathway under Diabetic Conditions. *Biomaterials* **2015**, *36*, 44–54. <https://doi.org/10.1016/J.BIOMATERIALS.2014.09.012>.
- (113) Liu, H.; Du, Y.; Wang, X.; Sun, L. Chitosan Kills Bacteria through Cell Membrane Damage. *Int. J. Food Microbiol.* **2004**, *95* (2), 147–155. <https://doi.org/10.1016/j.ijfoodmicro.2004.01.022>.

- (114) Sharma, S.; Soni, V. P.; Bellare, J. R. Chitosan Reinforced Apatite-Wollastonite Coating by Electrophoretic Deposition on Titanium Implants. *J. Mater. Sci. Mater. Med.* **2009**, *20* (7), 1427–1436. <https://doi.org/10.1007/s10856-009-3712-6>.
- (115) Peng, P.; Voelcker, N. H.; Kumar, S.; Griesser, H. J. Concurrent Elution of Calcium Phosphate and Macromolecules from Alginate/Chitosan Hydrogel Coatings. *Biointerphases* **2008**, *3* (4), 105–116. <https://doi.org/10.1116/1.3046123>.
- (116) Patz, T. M.; Doraiswamy, A.; Narayan, R. J.; Menegazzo, N.; Kranz, C.; Mizaikoff, B.; Zhong, Y.; Bellamkonda, R.; Bumgardner, J. D.; Elder, S. H.; et al. Matrix Assisted Pulsed Laser Evaporation of Biomaterial Thin Films. *Mater. Sci. Eng. C* **2007**, *27* (3), 514–522. <https://doi.org/10.1016/j.msec.2006.05.039>.
- (117) Chua, P. H.; Neoh, K. G.; Kang, E. T.; Wang, W. Surface Functionalization of Titanium with Hyaluronic Acid/Chitosan Polyelectrolyte Multilayers and RGD for Promoting Osteoblast Functions and Inhibiting Bacterial Adhesion. *Biomaterials* **2008**, *29* (10), 1412–1421. <https://doi.org/10.1016/j.biomaterials.2007.12.019>.
- (118) Shirosaki, Y.; Okamoto, K.; Hayakawa, S.; Osaka, A.; Asano, T. Preparation of Porous Chitosan-Siloxane Hybrids Coated with Hydroxyapatite Particles. *Biomed Res. Int.* **2015**, *2015*, 1–6. <https://doi.org/10.1155/2015/392940>.
- (119) Chen, W.; Shen, X.; Hu, Y.; Xu, K.; Ran, Q.; Yu, Y.; Dai, L.; Yuan, Z.; Huang, L.; Shen, T.; et al. Surface Functionalization of Titanium Implants with Chitosan-Catechol Conjugate for Suppression of ROS-Induced Cells Damage and Improvement of Osteogenesis. *Biomaterials* **2017**, *114*, 82–96. <https://doi.org/10.1016/j.biomaterials.2016.10.055>.
- (120) Henriksen, K.; Karsdal, M. A. Type I Collagen. In *Biochemistry of Collagens, Laminins and Elastin: Structure, Function and Biomarkers*; Elsevier Inc., 2016; pp 1–11. <https://doi.org/10.1016/B978-0-12-809847-9.00001-5>.
- (121) Makareeva, E.; Leikin, S. Collagen Structure, Folding and Function. In *Osteogenesis*

- Imperfecta: A Translational Approach to Brittle Bone Disease*; Elsevier Inc., 2013; pp 71–84. <https://doi.org/10.1016/B978-0-12-397165-4.00007-1>.
- (122) Nagai, M.; Hayakawa, T.; Fukatsu, A.; Yamamoto, M.; Fukumoto, M.; Nagahama, F.; Mishima, H.; Yoshinari, M.; Nemoto, K.; Kato, T. In Vitro Study of Collagen Coating of Titanium Implants for Initial Cell Attachment. *Dent. Mater. J.* **2002**, *21* (3), 250–260. <https://doi.org/10.4012/dmj.21.250>.
- (123) Geißler, U.; Hempel, U.; Wolf, C.; Scharnweber, D.; Worch, H.; Wenzel, K. W. Collagen Type I-Coating of Ti6Al4V Promotes Adhesion of Osteoblasts. *J. Biomed. Mater. Res.* **2000**, *51* (4), 752–760. [https://doi.org/10.1002/1097-4636\(20000915\)51:4<752::AID-JBM25>3.0.CO;2-7](https://doi.org/10.1002/1097-4636(20000915)51:4<752::AID-JBM25>3.0.CO;2-7).
- (124) Zhu, Y.; Liu, D.; Wang, X.; He, Y.; Luan, W.; Qi, F.; Ding, J. Polydopamine-Mediated Covalent Functionalization of Collagen on a Titanium Alloy to Promote Biocompatibility with Soft Tissues. *J. Mater. Chem. B* **2019**, *7* (12), 2019–2031. <https://doi.org/10.1039/c8tb03379j>.
- (125) Chang, W. J.; Ou, K. L.; Lee, S. Y.; Chen, J. Y.; Abiko, Y.; Lin, C. T.; Huang, H. M. Type I Collagen Grafting on Titanium Surfaces Using Low-Temperature Glow Discharge. *Dent. Mater. J.* **2008**, *27* (3), 340–346. <https://doi.org/10.4012/dmj.27.340>.
- (126) Kamata, H.; Suzuki, S.; Tanaka, Y.; Tsutsumi, Y.; Doi, H.; Nomura, N.; Hanawa, T.; Moriyama, K. Effects of PH, Potential, and Deposition Time on the Durability of Collagen Electrodeposited to Titanium. *Mater. Trans.* **2011**, *52* (1), 81–89. <https://doi.org/10.2320/matertrans.M2010311>.
- (127) Yang, X.; Jiang, B.; Huang, Y.; Tian, Y.; Chen, H.; Chen, J.; Yang, B. Collagen Nanofilm Immobilized on at Surfaces by Electrodeposition Method. *J. Biomed. Mater. Res. Part B Appl. Biomater.* **2009**, *90B* (2), 608–613. <https://doi.org/10.1002/jbm.b.31323>.

- (128) Brochier Salon, M. C.; Belgacem, M. N. Competition between Hydrolysis and Condensation Reactions of Trialkoxysilanes, as a Function of the Amount of Water and the Nature of the Organic Group. *Colloids Surfaces A Physicochem. Eng. Asp.* **2010**, *366* (1–3), 147–154. <https://doi.org/10.1016/j.colsurfa.2010.06.002>.
- (129) Vashist, S. K.; Lam, E.; Hrapovic, S.; Male, K. B.; Luong, J. H. T. Immobilization of Antibodies and Enzymes on 3-Aminopropyltriethoxysilane-Functionalized Bioanalytical Platforms for Biosensors and Diagnostics. *Chemical Reviews*. American Chemical Society November 12, 2014, pp 11083–11130. <https://doi.org/10.1021/cr5000943>.
- (130) Sharan, J.; Koul, V.; Dinda, A. K.; Kharbanda, O. P.; Lale, S. V.; Duggal, R.; Mishra, M.; Gupta, G.; Singh, M. P. Bio-Functionalization of Grade V Titanium Alloy with Type I Human Collagen for Enhancing and Promoting Human Periodontal Fibroblast Cell Adhesion – an in-Vitro Study. *Colloids Surfaces B Biointerfaces* **2018**, *161*, 1–9. <https://doi.org/10.1016/J.COLSURFB.2017.10.024>.
- (131) Marín-Pareja, N.; Salvagni, E.; Guillem-Martí, J.; Aparicio, C.; Ginebra, M. P. Collagen-Functionalised Titanium Surfaces for Biological Sealing of Dental Implants: Effect of Immobilisation Process on Fibroblasts Response. *Colloids Surfaces B Biointerfaces* **2014**, *122*, 601–610. <https://doi.org/10.1016/j.colsurfb.2014.07.038>.
- (132) Bady, M.; Jaffer, I. H.; Weitz, J. I.; Didar, T. F. An Omniphobic Lubricant-Infused Coating Produced by Chemical Vapor Deposition of Hydrophobic Organosilanes Attenuates Clotting on Catheter Surfaces. *Sci. Rep.* **2017**, *7* (1), 1–10. <https://doi.org/10.1038/s41598-017-12149-1>.
- (133) Bady, M.; Imani, S. M.; Weitz, J. I.; Didar, T. F. Lubricant-Infused Surfaces with Built-In Functional Biomolecules Exhibit Simultaneous Repellency and Tunable Cell Adhesion. *ACS Nano* **2018**, *12* (11), 10890–10902. <https://doi.org/10.1021/acsnano.8b03938>.

- (134) Hosseini, A.; Villegas, M.; Yang, J.; Badv, M.; Weitz, J. I.; Soleymani, L.; Didar, T. F. Conductive Electrochemically Active Lubricant-Infused Nanostructured Surfaces Attenuate Coagulation and Enable Friction-Less Droplet Manipulation. *Adv. Mater. Interfaces* **2018**, *5* (18). <https://doi.org/10.1002/admi.201800617>.
- (135) Kochkodan, V.; Tsarenko, S.; Potapchenko, N.; Kosinova, V.; Goncharuk, V. Adhesion of Microorganisms to Polymer Membranes: A Photobactericidal Effect of Surface Treatment with TiO<sub>2</sub>. *Desalination* **2008**, *220* (1–3), 380–385. <https://doi.org/10.1016/j.desal.2007.01.042>.
- (136) Gibbons, R. J.; Nygaard, M. Interbacterial Aggregation of Plaque Bacteria. *Arch. Oral Biol.* **1970**, *15* (12). [https://doi.org/10.1016/0003-9969\(70\)90031-2](https://doi.org/10.1016/0003-9969(70)90031-2).
- (137) Tuson, H. H.; Weibel, D. B. Bacteria-Surface Interactions. *Soft Matter*. Royal Society of Chemistry May 5, 2013, pp 4368–4380. <https://doi.org/10.1039/c3sm27705d>.
- (138) Xi, F.; Wu, J.; Lin, X. Novel Nylon-Supported Organic-Inorganic Hybrid Membrane with Hierarchical Pores as a Potential Immobilized Metal Affinity Adsorbent. *J. Chromatogr. A* **2006**, *1125* (1), 38–51. <https://doi.org/10.1016/j.chroma.2006.05.016>.
- (139) Nie, B.; Ao, H.; Zhou, J.; Tang, T.; Yue, B. Biofunctionalization of Titanium with Bacitracin Immobilization Shows Potential for Anti-Bacteria, Osteogenesis and Reduction of Macrophage Inflammation. *Colloids Surfaces B Biointerfaces* **2016**, *145*, 728–739. <https://doi.org/10.1016/J.COLSURFB.2016.05.089>.
- (140) Salehi-Nik, N.; Amoabediny, G.; Shokrgozar, M. A.; Mottaghy, K.; Klein-Nulend, J.; Zandieh-Doulabi, B. Surface Modification of Silicone Tubes by Functional Carboxyl and Amine, but Not Peroxide Groups Followed by Collagen Immobilization Improves Endothelial Cell Stability and Functionality. *Biomed. Mater.* **2015**, *10* (1). <https://doi.org/10.1088/1748-6041/10/1/015024>.

- (141) Madani, A.; Garakani, K.; Mofrad, M. R. K. Molecular Mechanics of Staphylococcus Aureus Adhesin, CNA, and the Inhibition of Bacterial Adhesion by Stretching Collagen. *PLoS One* **2017**, *12* (6). <https://doi.org/10.1371/journal.pone.0179601>.
- (142) Tanaka, M.; Nakahata, M.; Linke, P.; Kaufmann, S. Stimuli-Responsive Hydrogels as a Model of the Dynamic Cellular Microenvironment. *Polym. J.* **2020**, 1–10. <https://doi.org/10.1038/s41428-020-0353-6>.
- (143) Zouani, O. F.; Rami, L.; Lei, Y.; Durrieu, M. C. Insights into the Osteoblast Precursor Differentiation towards Mature Osteoblasts Induced by Continuous BMP-2 Signaling. *Biol. Open* **2013**, *2* (9), 872–881. <https://doi.org/10.1242/bio.20134986>.
- (144) Schweigert, N.; Zehnder, A. J. B.; Eggen, R. I. L. Chemical Properties of Catechols and Their Molecular Modes of Toxic Action in Cells, from Microorganisms to Mammals. Minireview. *Environ. Microbiol.* **2001**, *3* (2), 81–91. <https://doi.org/10.1046/j.1462-2920.2001.00176.x>.
- (145) Xu, J.; Strandman, S.; Zhu, J. X. X.; Barralet, J.; Cerruti, M. Genipin-Crosslinked Catechol-Chitosan Mucoadhesive Hydrogels for Buccal Drug Delivery. *Biomaterials* **2015**, *37*, 395–404. <https://doi.org/10.1016/j.biomaterials.2014.10.024>.
- (146) Ryu, J. H.; Lee, Y.; Kong, W. H.; Kim, T. G.; Park, T. G.; Lee, H. Catechol-Functionalized Chitosan/Pluronic Hydrogels for Tissue Adhesives and Hemostatic Materials. *Biomacromolecules* **2011**, *12* (7), 2653–2659. <https://doi.org/10.1021/bm200464x>.
- (147) GARTON, G. A.; WILLIAMS, R. T. Studies in Detoxication; the Fate of Catechol in the Rabbit and the Characterization of Catechol Monoglucuronide. *Biochem. J.* **1948**, *43* (2), 206–211. <https://doi.org/10.1042/bj0430206>.
- (148) Kamioka, H.; Sugawara, Y.; Honjo, T.; Yamashiro, T.; Takano-Yamamoto, T. Terminal Differentiation of Osteoblasts to Osteocytes Is Accompanied by Dramatic

- Changes in the Distribution of Actin-Binding Proteins. *J. Bone Miner. Res.* **2004**, *19* (3), 471–478. <https://doi.org/10.1359/JBMR.040128>.
- (149) Manivasagam, G.; Dhinasekaran, D.; Rajamanickam, A. Biomedical Implants: Corrosion and Its Prevention-A Review Super Hydrophilic Coatings View Project Coating on Implants for Biomedical Applications View Project Biomedical Implants: Corrosion and Its Prevention-A Review. *Recent Patents Corros. Sci.* **2010**, *2* (2), 40–54. <https://doi.org/10.2174/1877610801002010040>.
- (150) Hastings, G. W. Carbon Fibre Composites for Orthopaedic Implants. *Composites* **1978**, *9* (3), 193–197. [https://doi.org/10.1016/0010-4361\(78\)90345-2](https://doi.org/10.1016/0010-4361(78)90345-2).
- (151) Sarkar, D.; Mandal, S.; Reddy, B. S.; Bhaskar, N.; Sundaresh, D. C.; Basu, B. ZrO<sub>2</sub>-Toughened Al<sub>2</sub>O<sub>3</sub>-Based near-Net Shaped Femoral Head: Unique Fabrication Approach, 3D Microstructure, Burst Strength and Muscle Cell Response. *Mater. Sci. Eng. C* **2017**, *77* (1), 1216–1227. <https://doi.org/10.1016/j.msec.2017.03.123>.
- (152) Siqueira, J. T.; Cavalher-Machado, S. C.; Arana-Chavez, V. E.; Sannomiya, P. Bone Formation Around Titanium Implants in the Rat Tibia: Role of Insulin. *Implant Dent.* **2003**, *12* (3), 242–251. <https://doi.org/10.1097/01.ID.0000074440.04609.4F>.
- (153) Goodman, W. G.; Hori, M. T. Diminished Bone Formation in Experimental Diabetes. Relationship to Osteoid Maturation and Mineralization. *Diabetes* **1984**, *33* (9), 825–831. <https://doi.org/10.2337/diab.33.9.825>.
- (154) Li, X.; Ma, X.-Y.; Feng, Y.-F.; Ma, Z.-S.; Wang, J.; Ma, T.-C.; Qi, W.; Lei, W.; Wang, L. Osseointegration of Chitosan Coated Porous Titanium Alloy Implant by Reactive Oxygen Species-Mediated Activation of the PI3K/AKT Pathway under Diabetic Conditions. *Biomaterials* **2015**, *36*, 44–54. <https://doi.org/10.1016/j.biomaterials.2014.09.012>.

